© 2021. Published by The Company of Biologists Ltd | Development (2021) 148, dev193813. doi:10.1242/dev.193813

RESEARCH ARTICLE

Axial skeleton anterior-posterior patterning is regulated through feedback regulation between Meis transcription factors and retinoic acid

Alejandra C. López-Delgado[1,*], Irene Delgado[1], Vanessa Cadenas[1], Fátima Sánchez-Cabo[2] and Miguel Torres[1,‡]

ABSTRACT

Vertebrate axial skeletal patterning is controlled by co-linear expression of Hox genes and axial level-dependent activity of HOX protein combinations. MEIS transcription factors act as co-factors of HOX proteins and profusely bind to Hox complex DNA; however, their roles in mammalian axial patterning remain unknown. Retinoic acid (RA) is known to regulate axial skeletal element identity through the transcriptional activity of its receptors; however, whether this role is related to MEIS/HOX activity remains unknown. Here, we study the role of Meis in axial skeleton formation and its relationship to the RA pathway in mice. Meis elimination in the paraxial mesoderm produces anterior homeotic transformations and rib mis-patterning associated to alterations of the hypaxial myotome. Although Raldh2 and Meis positively regulate each other, *Raldh2* elimination largely recapitulates the defects associated with Meis deficiency, and Meis overexpression rescues the axial skeletal defects in *Raldh2* mutants. We propose a Meis-RA-positive feedback loop, the output of which is Meis levels, that is essential to establish anterior-posterior identities and patterning of the vertebrate axial skeleton.

KEY WORDS: Embryo patterning, Homeodomain, Homeotic transformation, Myogenesis, Skeletal patterning, Vertebral patterning

INTRODUCTION

Anterior-posterior (AP) patterning is an essential feature of the bilaterian body plan and its mechanisms have been extensively studied. Segmental epithelial sacs known as somites emerge from the paraxial mesoderm as it is produced and these sacs progressively incorporate to the AP axis. The initially homogeneous somites later subdivide into compartments, including the sclerotome, which is the precursor of the vertebrae and ribs, and the myotome, which is the precursor of the skeletal muscles (Musumeci et al., 2015). Crosstalk from the myotome to the sclerotome is essential for sclerotome patterning and in particular for rib specification and patterning (Vinagre et al., 2010).

[1]Cardiovascular Development Program, Centro Nacional de Investigaciones Cardiovasculares (CNIC), Madrid 28003, Spain. [2]Bioinformatics Unit, Centro Nacional de Investigaciones Cardiovasculares (CNIC), Madrid 28003, Spain. *Present address: Center for Regenerative Therapies, TU Dresden, Dresden 01307, Germany.

‡Author for correspondence (mtorres@cnic.es)

A.C.L.-D., 0000-0003-2187-3938; I.D., 0000-0002-0493-8261; F.S.-C., 0000-0003-1881-1664; M.T., 0000-0003-0906-4767

Handling Editor: Benoit Bruneau
Received 9 June 2020; Accepted 20 November 2020

An important breakthrough in understanding AP axis patterning was the identification of Hox mutants in *Drosophila*, which cause the transformation of one part of the body into another: a phenomenon known as homeotic transformation (Lewis, 1978). Hox genes are conserved in evolution and appear to be organized in genetic complexes in most animals (Duboule and Dolle, 1989; Sanchez-Herrero et al., 1985). Mutations in Hox genes in different species produce AP homeotic transformations, which in mammals is best exemplified in the hindbrain and in the axial skeleton (Krumlauf, 1994).

Hox gene transcription is activated sequentially in axial precursors during gastrulation (Deschamps et al., 1999). As cells derived from these precursors colonize the different AP segments, they carry the successive Hox expression combinations to the progressively forming body axis, resulting in an AP nested patterns (Alexander et al., 2009). Thus, temporal information is translated into spatial domains during axial elongation (Deschamps and Duboule, 2017).

HOX proteins bind DNA through a highly conserved 60 amino acid region called the homeodomain (McGinnis et al., 1984). HOX proteins alone show limited DNA-binding ability, but they gain specificity and affinity for target sequences through interactions with co-factors of the PBC and MEINOX families, both belonging to the three amino acid loop extension (TALE) class of homeodomains (Mann and Affolter, 1998). PBC and MEINOX proteins form heterodimers and heterotrimers with HOX proteins, conferring them with increased target sequence selectivity and affinity (Merabet and Mann, 2016). Mutation of single members of the PBC and MEINOX families in *Drosophila* show AP phenotypes compatible with a generalized Hox gene loss of function, without affecting *Hox* AP expression (Chan et al., 1994; Rieckhof et al., 1997). In mammals, redundancy of the PBC (four members) and MEINOX (five members) families has hampered the study of their roles in axial skeletal patterning. Although knowledge has been obtained from Pbx mutants in zebrafish and mouse, indicating essential roles in axial skeleton patterning (Capellini et al., 2008; Popperl et al., 2000; Selleri et al., 2001), the role of Meis genes in this context remains unexplored.

MEIS proteins directly bind HOX proteins encoded by paralogs 9-13 (Shen et al., 1997) and form DNA-bound heterotrimeric complexes with PBX and HOX proteins encoded by paralogs 1-10 (Chang et al., 1996). The repertoire of MEIS-, PREP- and PBX-binding sites revealed by ChIP-seq analysis in E11.5 mouse embryos identified HOX and HOX-PBC binding sites as the preferred sites for MEIS binding, above the MEIS-only binding sites, suggesting that MEIS factors are strongly dedicated to interactions with HOX and PBX proteins (Penkov et al., 2013). In addition, a large number of MEIS-binding sites was found within the Hox gene complexes, which suggested that, in addition to their HOX co-factor role, they may regulate Hox gene transcription.

Development (2021) 148, dev193813. doi:10.1242/dev.193813

Studies in zebrafish (Choe et al., 2014) and mouse (Amin et al., 2015) embryos indeed show that some of these binding sites represent Hox auto-regulatory elements that are active in the neural tube, and Hox transcription regulation by MEIS factors has been demonstrated in neural tube patterning (Dibner et al., 2001; Vlachakis et al., 2001; Waskiewicz et al., 2001). MEIS elimination or overexpression also affects Hox gene expression during limb skeletal patterning (Delgado et al., 2020; Mercader et al., 1999, 2009; Rosello-Diez et al., 2014); however, this aspect has not been studied in axial skeleton patterning.

An important pathway connecting MEIS, HOX and axial patterning is that of vitamin A. The active form of vitamin A, retinoic acid (RA), regulates gene expression during embryonic development by binding to nuclear receptors RARα, RARβ or RARγ (Rhinn and Dolle, 2012). Meis genes have been identified in screens for RA targets (Berenguer et al., 2020; Oulad-Abdelghani et al., 1997) and respond to RA fluctuations *in vivo* (Mercader et al., 2000; Yashiro et al., 2004). RA excess produces axial skeleton alterations and modifies the Hox AP expression domains (Kessel and Gruss, 1991) and mutations in RA-receptor genes result in homeotic transformations; however, the mechanism by which this takes place is not clear. Although RAR binding sites have been described in Hox complexes (Marshall et al., 1996), and RA administration *in vitro* regulates Hox gene transcription (Deschamps et al., 1987), RA administration *in vivo* can lead to axial skeleton homeotic transformations without changes in Hox expression (Kessel, 1992) and changes in Hox expression in Rar-deficient mice have not been reported.

Here, we study the role of MEIS factors in axial skeleton formation and its relationship to the RA pathway by characterizing mouse genetic models of *Meis1*, *Meis2* and *Raldh2* (the synonym for *Aldh1a2*). We dissect the regulatory and functional relationships between Meis genes, Hox genes and *Raldh2*, and formulate a new model that explains the ability of RA to produce homeotic transformations without modifying Hox expression.

RESULTS

Meis gene expression during anterior-posterior axial patterning of the mouse embryo

We studied the mRNA expression pattern of *Meis1* and *Meis2*: the two Meis genes extensively expressed in paraxial and lateral mesoderm (Fig. 1). We detected the earliest expression of *Meis2* in early-streak stage embryos in a posterior region of the embryo close to the boundary with the extra-embryonic region (Fig. 1H). This expression extends distally and anteriorly as development progresses (Fig. 1I); at the early-headfold stage, an anterior stripe of *Meis2* transcripts was found bilaterally close to the extra-embryonic region, and continuous with its posterior expression (Fig. 1J). At late-headfold stage, *Meis2* started to disappear from the posterior region (Fig. 1K) and at E8, the posterior embryonic bud was devoid of *Meis2* transcripts (Fig. 1L). *Meis1* expression started slightly later than *Meis2*, being first detected at the late-streak stage, bilaterally in the mesoderm close to the extra-embryonic region (Fig. 1B), and at the early-headfold stage, forming a stripe of expression similar to the *Meis2* anterior stripe at this stage (Fig. 1C). Both *Meis1* and *Meis2* expression domains extend posteriorly into the lateral plate mesoderm at the late-headfold stage (Fig. 1D,K), but high levels of *Meis1* transcripts were never observed in the posterior embryonic bud. Finally, at E8 *Meis1* and *Meis2* expression patterns converge to a similar domain, being strongly expressed in paraxial and lateral plate mesoderm up to the pharyngeal region (Fig. 1E,L). At this stage, expression of both genes is excluded from the posterior embryonic bud, whereas it appears in the presomitic mesoderm and adjacent regions precursor to the lateral plate mesoderm. This expression pattern is maintained at later stages, indicating that as new precursors from the posterior bud incorporate to the presomitic area, they activate *Meis1* and *Meis2*, and this activity persists as they differentiate into paraxial and lateral plate mesoderm. To determine the early activation pattern of *Meis1* and *Meis2* in the embryonic germ layers, we studied Meis mRNA and protein distribution in sections (Fig. 1). Detection of MEIS proteins in sections with an antibody that recognizes the majority of embryonic isoforms, but does not discriminate between MEIS1 and MEIS2, shows early expression in all three germ layers at early allantoic bud stage (Fig. 1G,N). Sections of the RNA *in situ* hybridization of both genes, showed that *Meis1* expression was not detected in the epiblast/ectoderm (Fig. 1F), while *Meis2* expression affected the three germ layers (Fig. 1M). This result suggests *Meis2* is activated in epiblast cells and its expression persists as they gastrulate to contribute to mesoderm. The early *Meis2* expression pattern thus resembles the activation pattern of Hox genes.

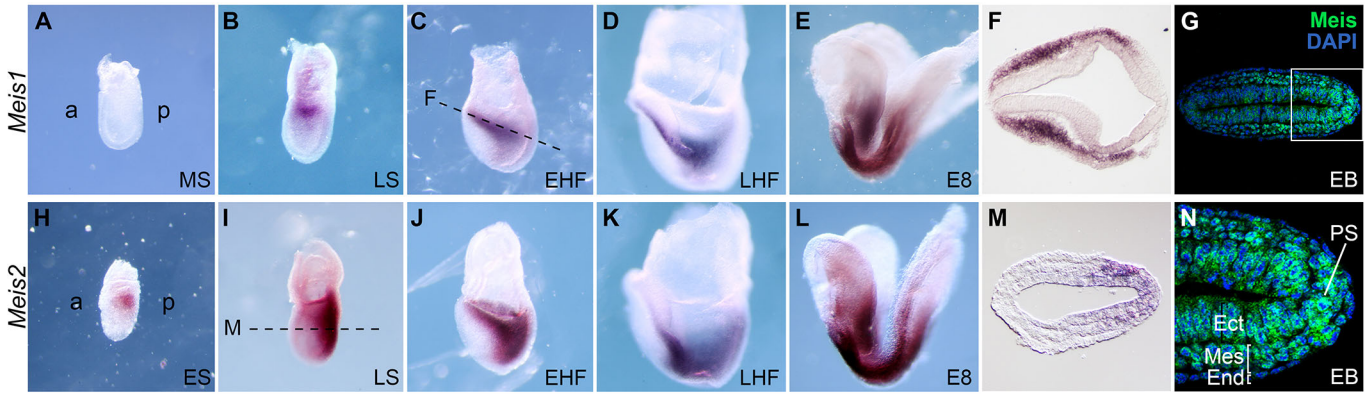

Fig. 1. Meis expression pattern in early mouse embryo development. Whole-mount mRNA *in situ* hybridization of *Meis1* (A-E) and *Meis2* (H-L) from E7 to E8. (F,M) Transverse sections showing *in situ* hybridization for *Meis1* and *Meis2* mRNA, respectively. The plane of the section is indicated by dashed lines in C and I. (G) Immunostaining against both Meis1 and Meis2 on longitudinal sections of an EB embryo across the PS. (N) Magnification of the region marked in G with the three germ layers indicated. a, anterior; p, posterior; MS, mid-streak; LS, late-streak; EHF, early headfold; LHF, late headfold; ES, early-streak; EB, early allantoic bud; PS, primitive streak; Ect, ectoderm; Mes, mesoderm; End, endoderm. All images show anterior to the left and posterior to the right.

Development (2021) 148, dev193813. doi:10.1242/dev.193813

Meis loss of function produces axial skeletal defects, including anterior-posterior homeotic transformations

We used conditional deletion of *Meis1* and *Meis2* and studied the mutant skeletal pattern. We first studied the consequences of *Meis2* deletion using different Cre alleles that allow dissecting the putative specific functions of *Meis2* early expression. Deletion of a $Meis2^{flox}$ allele with $Sox2^{Cre}$ leads to *Meis2* elimination in the epiblast. Lethality of $Sox2^{Cre};Meis2^{flox/flox}$ embryos around E14.5-E15.5 due to cardiac defects did not allow us to study the pattern at later stages; however, the general vertebral formula could be determined at E14.5. We observed defects at the occipital-cervical transition, where the first cervical vertebra (C1 or atlas) was fused to the exoccipital bone (n=14/14) and in its ventral part showed a position and shape that resemble the exoccipital bone, while its dorsal part was not formed (Fig. 2A,B; Fig. S1; Table S1A). These changes correlated with a change in the shape of the second vertebra (C2 or axis), which acquired a C1-like morphology (n=13/14) (Fig. 2A,B; Fig. S1). With low penetrance, the C3 vertebra presented a morphology that resembles C2 (n=2/14). These observations are compatible with an anterior homeotic transformation of the cervical vertebrae. In addition, disconnected isolated elements often appeared (arrowhead in Fig. 2B; Fig. S1), suggesting segmentation problems are also present in this region. Outside the axial skeleton, we observed a vestigial otic capsule in the mutants.

In the thoracic region, the most prominent defect was rib, rib-sternum attachment and sternum mispatterning (Fig. 2D,E). We observed failures in sternum fusion, rib bifurcations, fusions and alteration of the sternal/floating rib formula. The gain of a rib in the first lumbar vertebra (L1) in some specimens (n=4/14) and the tendency to reduction of the first rib (R1) suggests the anterior transformations observed in the cervical region may also affect the thoracic region (Fig. 2B). More caudal regions did not show any defects.

To investigate whether *Meis2* activity in the epiblast is involved in the observed defects, we combined the $Meis2^{flox}$ allele with $Mesp1^{Cre}$ to eliminate *Meis2* from the nascent mesoderm. Although *Mesp1* activates in the early embryo in a similar pattern to *Meis2*, because of the time lag between Cre expression and effective recombination, the recombination pattern of $Mesp1^{Cre}$ affects only the mesoderm and it does so down to the forelimb level (Saga et al., 1999). As occurred in $Sox2^{Cre};Meis2^{flox/flox}$ mice, lethality due to cardiac defects allowed us to study the phenotype only until E14.5. In the $Mesp1^{Cre}$ model, we observed lower penetrance, but the same type and distribution of defects found in the $Sox2^{Cre}$ model, except for the reduction of R1 and the otic capsule defects (Fig. 2C,F; Fig. S1; Table S1A).

To further dissect the specific tissues in which *Meis2* activity is required during early embryogenesis, we studied a third model in which we deleted $Meis2^{flox}$ using $Dll1^{Cre}$, a line that recombines the mesoderm in the presomitic region (Wehn et al., 2009), i.e. at a later

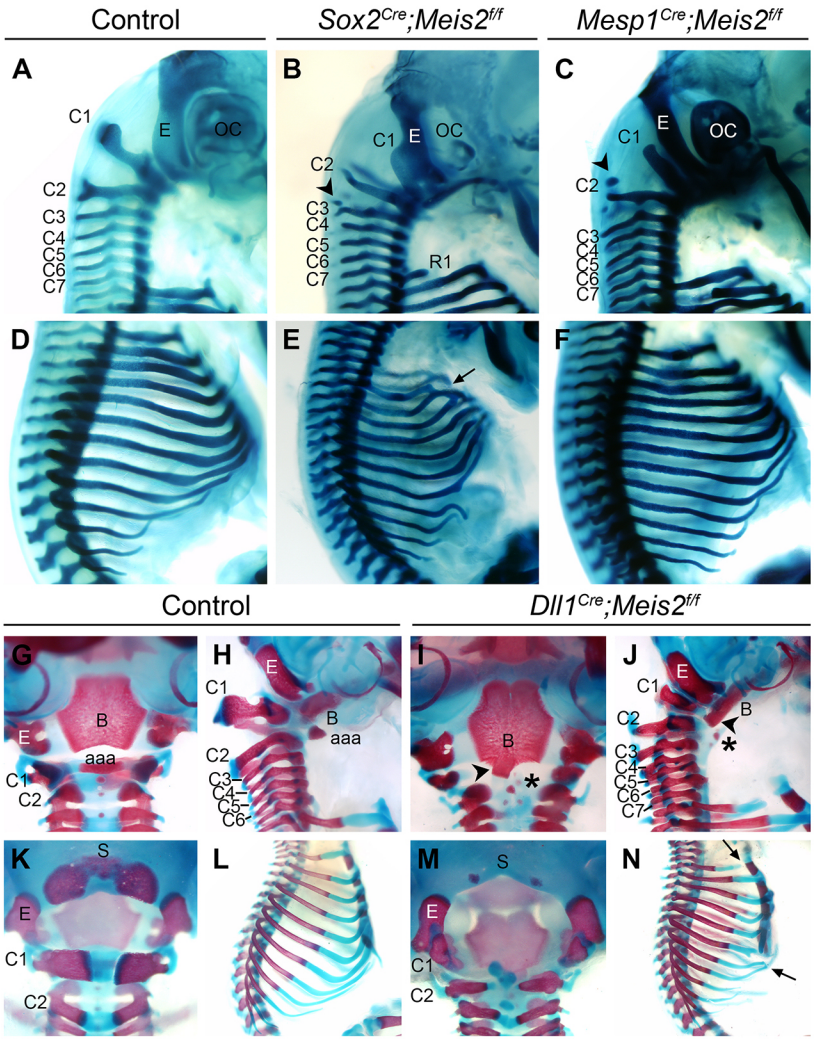

Fig. 2. Skeletal defects in conditional *Meis2* mutant fetuses using different Cre alleles. (A-F) Victoria Blue-stained skeletal preparations of E14.5 fetuses. The cervical region is shown for control (A), $Sox2^{Cre};Meis2^{f/f}$ (B) and $Mesp1^{Cre};Meis2^{f/f}$ (C) fetuses. Arrowheads in B and C indicate disconnected chondrogenic condensations. The thoracic region is shown for control (D), $Sox2^{Cre};Meis2^{f/f}$ (E) and $Mesp1^{Cre};Meis2^{f/f}$ (F) fetuses. Arrows in E and N indicate rib defects. (G-N) Alizarin Red/Alcian Blue-stained skeletal preparations of E18 control (G,H,K,L) and $Dll1^{Cre};Meis2^{f/f}$ (I,J,M,N) fetuses. The occipital region is shown in ventral (G,I), lateral (H,J) and dorsal (K,M) views. (L,N) Lateral views of the thoracic region. Arrowheads in I and J indicate fusion between the basioccipital and the aaa. Asterisks in I and J indicate ectopic aaa formed on C2. aaa, anterior arch of the atlas; B, basioccipital; C, cervical vertebra; E, exoccipital; OC, otic capsule; R, rib; S, supraoccipital.

Development (2021) 148, dev193813. doi:10.1242/dev.193813

step of mesodermal allocation than does *Mesp1*^{Cre}. *Dll1*^{Cre};*Meis2*$^{flox/flox}$ mice survive to adulthood, allowing a full assessment of the skeletal pattern at the end of gestation. In this model, we observed similar defects to those previously observed in the *Sox2*^{Cre} and *Mesp1*^{Cre} models in the occipital, cervical and thoracic regions (Figs 2G-N and 3M; Fig. S1; Table S1A). In addition, we observed a defect in supraoccipital ossification (Figs 2K,M and 3M) and fusions between the basioccipital and the anterior arch of the atlas (aaa) (Fig. 2G,I; Fig. S1 and Fig. 3M), which could not be determined at earlier stages because these bones form late in gestation. Again, we did not detect the formation of a rib in L1, suggesting this phenotype requires an early deletion of *Meis2*.

The irrelevance of early *Meis2* expression for most aspects of axial patterning is not due to compensatory activation of *Meis1*, as we detected no ectopic *Meis1* mRNA expression in early *Sox2*^{Cre};*Meis2*$^{flox/flox}$ embryos (Fig. S2). These results indicate that the expression of *Meis2* in the epiblast and early nascent mesoderm is to a large extent dispensable for its functions in axial skeletal patterning, although it might be needed for a proper specification of the thoracic-to-lumbar transition.

Next, to determine whether *Meis1* and *Meis2* cooperate in axial patterning, we combined *Meis1* and *Meis2* mutant alleles. Combining *Meis1* and *Meis2* deletion is not possible using the *Sox2*^{Cre} or the *Mesp1*^{Cre} deleters, owing to lethality of double heterozygous mice. We therefore used the *Dll1*^{Cre} line for these experiments. The defects observed in the allelic series generated affected the same skeletal elements that were altered in the *Meis2* mutant models (Fig. 3) and the type of defects were similar, with anterior transformations of C1-C3 (Fig. 3G-I,M; Fig. S3; Table S1B,C) and defects in the occipital bones that either did not

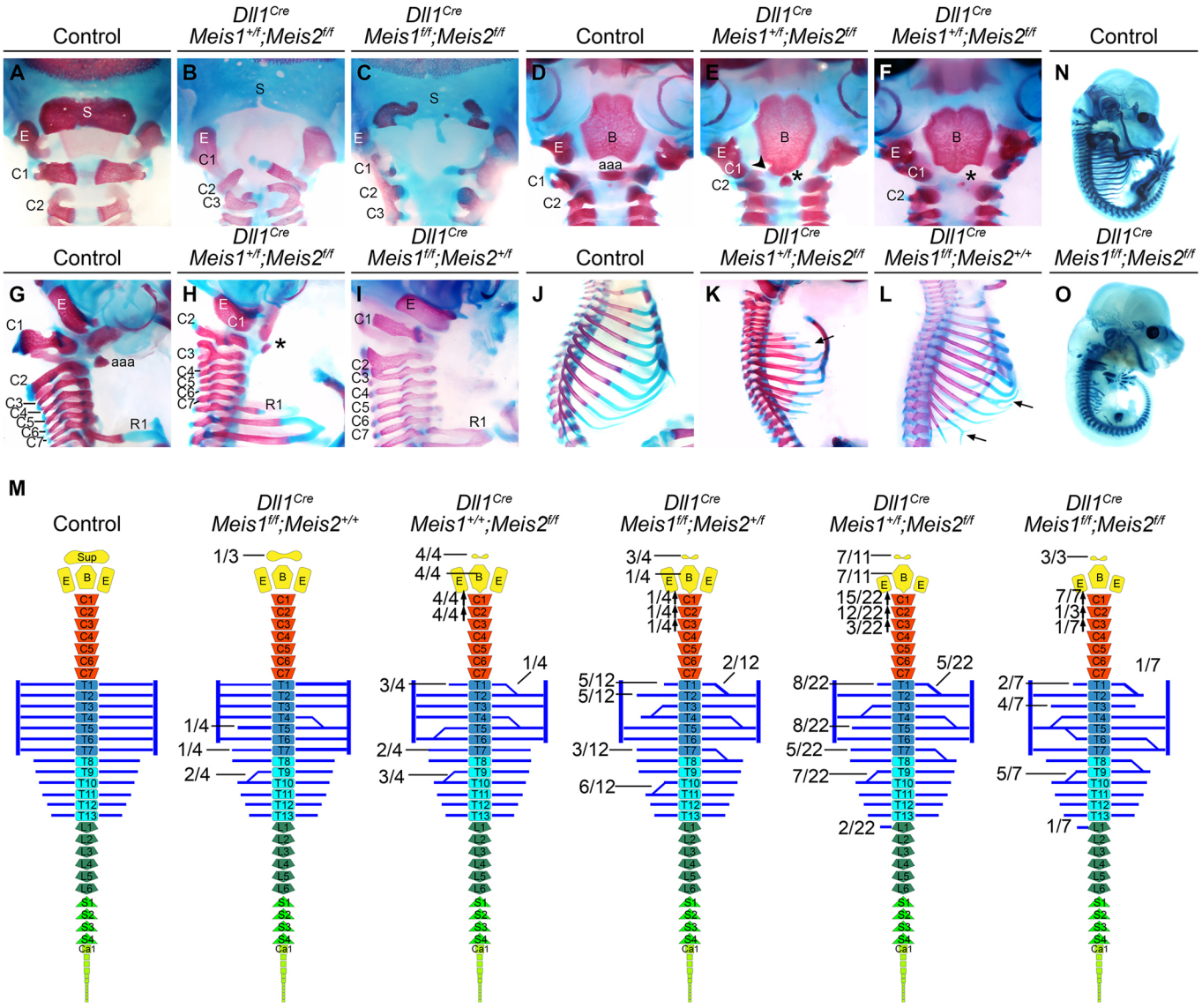

Fig. 3. Skeletal defects in *Meis1* and *Meis2* loss-of-function mice using *Dll1*^{Cre}. (A-L) Alizarin Red/Alcian Blue-stained skeletal preparations of E18.5 fetuses, control or mutant for different combinations of *Meis1* and *Meis2* floxed alleles, and *Dll1*^{Cre}. The occipital region of control and mutant combinations is shown in dorsal (A-C), ventral (D-F) and lateral (G-I) views. (J-L) Lateral views of the thoracic region. The arrowhead in E indicates a fusion between the basioccipital and aaa. Asterisks indicate ectopic aaa formed on C2. Arrows in K and L indicate rib defects. (M) Schematic representation of the axial skeleton defects of the different genotypes analyzed and their frequencies. Arrows pointing upwards indicate apparent anterior homeotic transformations. (N,O) Victoria Blue-stained skeletal preparations of E14.5 fetuses. aaa, anterior arch of the atlas; B, basioccipital; C, cervical vertebra; E, exoccipital; R, rib; S, supraoccipital.

Development (2021) 148, dev193813. doi:10.1242/dev.193813

form or appeared fused to the C1 or C2 element (Fig. 3A-I,M; Fig. S3; Table S1B,C). In the thoracic region, we also detected rib fusions and defects in rib-sternum attachment (Fig. 3J-M; Table S1B,C). Although we found two cases of extra ribs on L1, one case was also found in controls, suggesting this observation was nonspecific. In general, skeletal defects become more severe as the number of Meis alleles deleted increases, with the absence of *Meis2* being more detrimental than absence of *Meis1* (Fig. 3M; Fig. S3; Table S1B,C). However, for some aspects of the phenotype, E18.5 $Dll1^{Cre};Meis1^{flox/flox};Meis2^{flox/flox}$ specimens appeared less affected in comparison with $Dll1^{Cre};Meis1^{+/flox};Meis2^{flox/flox}$ specimens, which was paradoxical. However, we observed, that the viability of $Dll1^{Cre};Meis1^{flox/flox};Meis2^{flox/flox}$ mice at E18.5 was 37%, which suggested that specimens of this genotype at E18.5 represent escapers; thus, missing specimens could be more affected than appreciated. We then studied the phenotype of $Dll1^{Cre};Meis1^{flox/flox};Meis2^{flox/flox}$ fetuses at E14.5, when viability of double mutants was 67%, and observed a fraction of embryos with defects compatible with those observed at E18.5 and, in addition, we found very strongly affected fetuses in which all the cervical vertebrae fused, there was no apparent development of occipital condensations, and there were widespread rib fusions and truncations (Fig. 3N,O). In addition to the axial skeleton, defects in the limb skeleton were obvious in $Dll1^{Cre};Meis1^{flox/flox};Meis2^{flox/flox}$ fetuses (Fig. 3N,O) and have been independently reported (Delgado et al., 2020).

Hox mRNA axial expression in Meis mutants

Although defects in vertebral segmentation or overt rib deformations have not been described in Hox mutants, the AP specification defects observed in the occipital and cervical regions are very similar to those observed in the mutants of Hox paralog groups 3-5, and some of the rib cage defects are similar to those found in paralog groups 5-9 (Horan et al., 1995; Jeannotte et al., 1993; Manley and Capecchi, 1997; McIntyre et al., 2007). These coincidences and the previous reports of MEIS proteins binding to Hox gene clusters (Amin et al., 2015; Penkov et al., 2013) prompted us to study the Hox mRNA expression pattern in Meis mutants. We did not detect alterations of Hox expression initiation or definitive anterior expression borders in the paraxial mesoderm in either $Sox2^{Cre};Meis2^{flox/flox}$ or in $Dll1^{Cre};Meis1^{flox/flox};Meis2^{flox/flox}$ embryos (Fig. 4A,B). These results indicate that eliminating *Meis2* function with $Sox2^{Cre}$ or *Meis1* and *Meis2* $Dll1^{Cre}$ does not modify Hox gene expression patterns and therefore, the phenotypes observed in these models do not relate to a role for Meis genes in regulating Hox gene transcription in the paraxial mesoderm. To study the generality of these observations, we combined simultaneous maternal and paternal deletion of $Meis1^{flox/flox}$ and $Meis2^{flox/flox}$ alleles, using the maternal deleter $Zp3^{Cre}$ and the paternal deleter $Stra8^{Cre}$ (Fig. S4). Using this approach, we were able to completely eliminate *Meis1* and *Meis2* zygotic expression. Such embryos die around E9 with profound alterations of cardiac development; however, this allowed us to study early Hox expression patterns. Although previous reports in embryos at E9.5 or later stages have described paralog group Hox3 gene expression starting at somite 5 (Alexander et al., 2009), we found that in control embryos of up to 10 somites, expression of the Hox3 paralog group extended from somite 2-3 into more posterior somites (Fig. 4C, Fig. S5). In embryos of 12 somites, the most anterior expressing somite is somite 3-4, while in embryos of 15 or more somites, expression starts at somite 5. These observations show transient Hox3 gene expression in occipital somites and a later progressive posteriorization towards their definitive expression domain. This expression pattern is consistent with the observation that the occipital region, which mostly originates from somites 1-4, is strongly affected in Hox3 mutants. The defects present in Hox3 mutants in fact strongly affect the supraoccipital bone, which is exclusively contributed to by somites 1 and 2 (Huang et al., 2001; Muller and O'Rahilly, 1994). Meis mutant embryos showed a normal Hox3 group gene expression in the paraxial mesoderm of embryos of 4-10 somites (Fig. 4C, Fig. S5). In more advanced stages, although counting somites was very difficult in mutant embryos of 15-20 somites, due to the developmental abnormalities, we concluded that the expression patterns in the paraxial mesoderm were either normal or anteriorized by 1-2 somites (Fig. 4C, Fig. S5). In contrast, the anterior border of expression in the neural tube appeared clearly posteriorized (Fig. 4C, Fig. S5). The study of the expression of *Hoxd4* showed similar results, with a transient early expression starting at somite 4 and later becoming restricted to its definitive anterior border at somite 6. In mutants, *Hoxd4* expression was similar at early stages and appeared anteriorized to somite 4-5 at later stages. A posteriorization of *Hox* mRNA expression in the neural tube was again evident (Fig. 4C, Fig. S5). Most likely, the failure of the mutants to relocate Hox expression to more posterior somites at late stages does not indicate a direct role for MEIS proteins in regulating Hox gene expression, but a general blockade in development of Meis double knockout (DKO) embryos beyond the somite 7 stage. In fact, Meis DKO embryos do not undergo turning, body wall folding or neural tube closure, morphologically resembling E8.5 embryos at E9. The fact that no alterations were observed upon deletion with $Dll1^{Cre}$ support this conclusion. We therefore conclude that transcriptional regulation of Hox genes is not involved in MEIS protein-mediated regulation of axial skeleton patterning.

Meis gene activity is required for hypaxial myotomal development

To identify the molecular mechanism underlying the skeletal phenotypes observed, we performed a transcriptomic analysis of E9 $Dll1^{Cre};Meis1^{flox/flox};Meis2^{flox/flox}$ embryos. To discriminate between alterations during the somite differentiation phase and early patterning defects, we separately analyzed the anterior region containing the first 10-12 somites and the posterior region, including the rest of the somites and the posterior embryonic bud. We identified 9 upregulated genes and 25 downregulated genes in the analysis of the anterior region, whereas in the posterior region there were 58 upregulated and 58 downregulated genes (Fig. S6A,B). Regulatory pathway analysis showed that 'skeletal and muscular system development' appears as the top tissue-specific altered class (Fig. S6C). Differences in other processes, such as cell death, cell-to-cell interactions, cell assembly and organization, were also found in this analysis (Fig. S6C). No alterations were found in Hox gene expression, which confirmed the results observed in the Hox mRNA *in situ* analysis.

We then focused on the *in situ* analysis of genes involved in somite development found altered in the RNAseq analysis and in additional genes relevant to somite patterning. When comparing the expression pattern of this set of genes between control and $Dll1^{Cre};Meis1^{flox/flox};Meis2^{flox/flox}$ embryos, we found that a set of genes expressed and/or involved in hypaxial myotomal development were downregulated in the hypaxial region of the mutants (Fig. 5), including *Eya1* (Grifone et al., 2007) (Fig. 5A,B), *Sim1* (Ikeya and Takada, 1998) (Fig. 5C,D), *Shisa2* (Nagano et al., 2006) (Fig. 5E,F) and *Pax3* (Tremblay et al., 1998) (Fig. 5G,H). Regarding sclerotome markers, we found no alteration of *Pax1* expression (Fig. 5I,J);

Development (2021) 148, dev193813. doi:10.1242/dev.193813

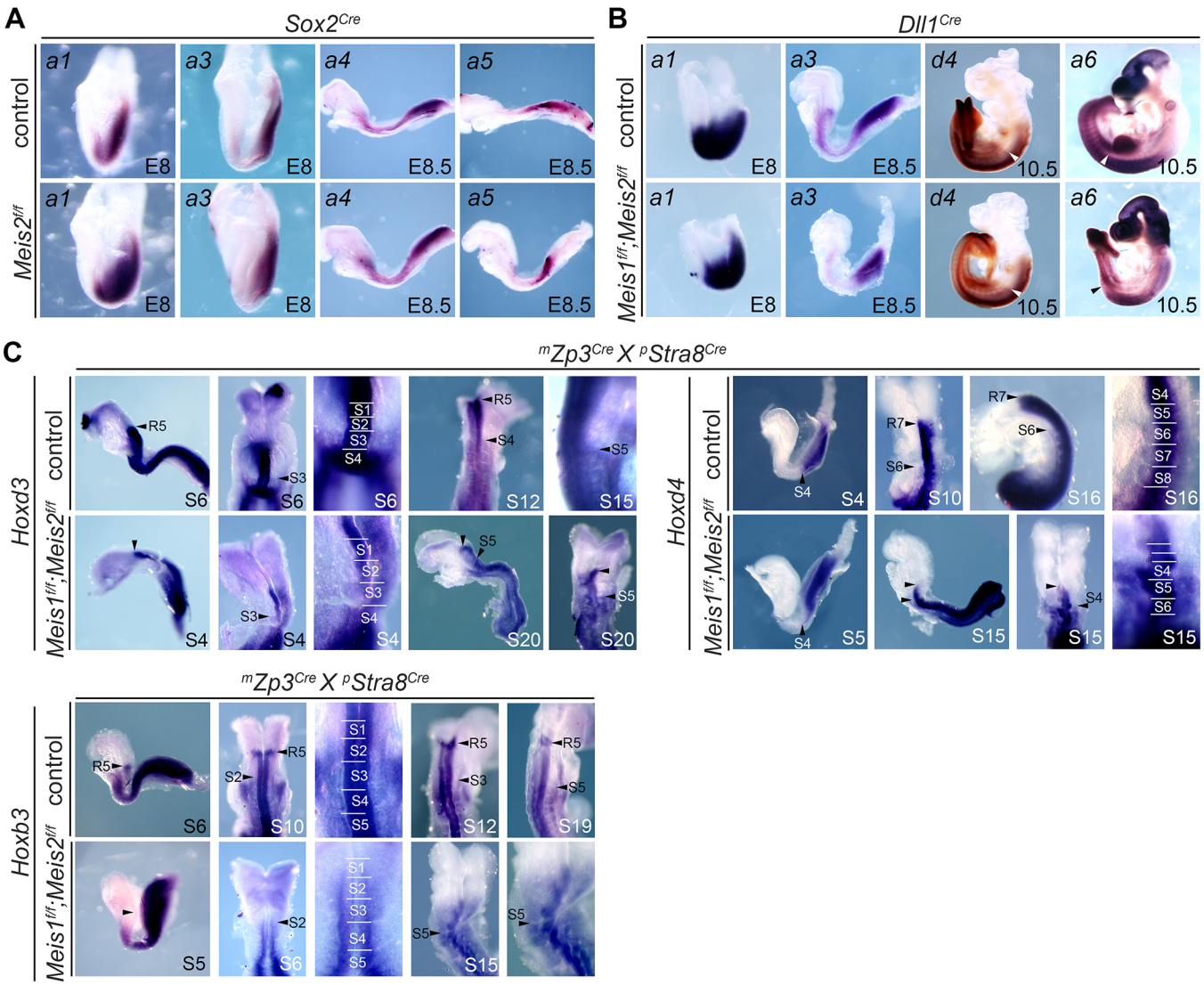

Fig. 4. Hox gene mRNA expression patterns in Meis loss-of-function mutants. (A) mRNA *in situ* hybridization of the indicated Hox genes in E8-E8.5 control and *Sox2*^{Cre}-recombined *Meis2* conditional mutant embryos. (B) mRNA *in situ* hybridization of the indicated Hox genes in E8-E10.5 control and *Dll1*^{Cre}-recombined *Meis1* and *Meis2* conditional mutant embryos. (C) mRNA *in situ* hybridization of the indicated Hox genes in control and double-floxed *Meis1* and *Meis2* embryos derived from *Zp3*^{Cre} mothers and *Stra8*^{Cre} fathers. Arrowheads in B and C indicate the anterior-most boundaries of Hox gene expression. In C, anterior-most somites or rhombomeres showing expression are indicated by arrowheads next to the letters S and R, respectively. S# in the bottom right of each image indicates the somite stage of the embryo shown.

however, an abnormal expression pattern of *Pax9* was observed in sclerotomes of the cervical region, which appeared incorrectly segmented (Fig. 5K,L).

Crosstalk between the myotome and sclerotome is essential for proper rib patterning and mice deficient for the myogenic factors MYF5 (Braun et al., 1992), MRF4 (Zhang et al., 1995) or myogenin (Vivian et al., 2000) show rib defects that resemble those described here in Meis mutants. Therefore, we next studied the main myogenic factors. Expression of *Myf5* appears first in the epaxial somite at E8, followed by *Mrf4* and *Myog* at E9, later extending hypaxially caudal to the forelimb at E10.5 (Fig. 5M-R). In mutant mice, the early epaxial expression of *Myf5* shows incomplete segmentation, whereas at E10.5, expression in myotomes anterior to the forelimb extends ventrally and appears as a continuous band between adjacent somites in a pattern that is not detected in control embryos (Fig. 5M,N). Both *Mrf4* and *Myog* show mis-segmented and bifurcating patterns in mutant embryos (Fig. 5O-R). In addition, the ventral hypaxial extension of the expression domain was reduced, as observed before for other hypaxial markers. In contrast, defects in the early expression of *Myog* at E9 are not as evident as for *Myf5*. *Myod1* shows as well a disorganized and spread expression in cervical myotomes of mutants, whereas hypaxial extension of the expression is also defective in more caudal myotomes (Fig. 5S-T).

We finally studied *Fgf4* and *Fgf6*, which are involved in myogenesis through their expression in the medial myotome (Grass et al., 1996). We found that expression of *Fgf4* and *Fgf6* appeared highly reduced in mutant embryos (Fig. 5U-X).

In summary, re-segmentation of the paraxial mesoderm appears impaired in Meis mutants, with defects in the separation of adjacent sclerotomal/myotomal domains and bifurcated myogenic domains. These defects affect mainly the cervical region, although defects were also seen sometimes in the interlimb region. During further myotome development, a defect in myogenic Fgf gene expression was found and the hypaxial developmental program seemed especially affected, with a failure in hypaxial myotomal migration in correlation with an inability to properly activate *Pax3* expression.

Development (2021) 148, dev193813. doi:10.1242/dev.193813

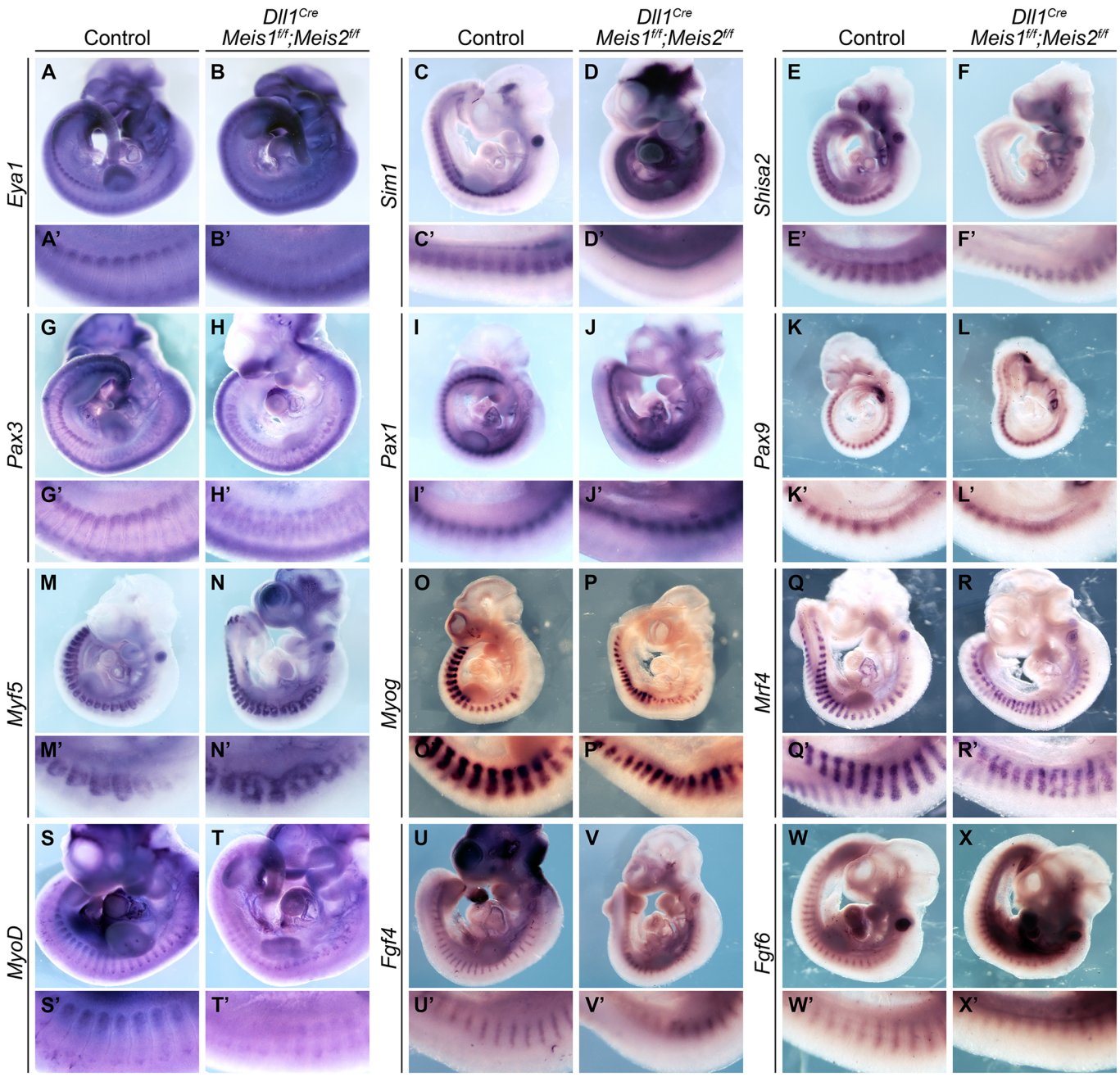

Fig. 5. Expression analysis of genes involved in somite development in Meis mutants. Images show whole-mount *in situ* mRNA hybridization in E10.5 embryos in control and *Dll1*^{Cre};*Meis1*$^{f/f}$;*Meis2*$^{f/f}$ embryos. (A,B) *Eya1*, (C,D) *Sim1*, (E,F) *Shisa2*, (G,H) *Pax3*, (I,J) *Pax1*, (K,L) *Pax9*, (M,N) *Myf5*, (O,P) *Myog*, (Q,R) *Mrf4*, (S,T) *Myod1*, (U,V) *Fgf4* and (W,X) *Fgf6*. (A′-X′) Magnification of the trunk region of the corresponding image.

To study whether any of the skeletal or myogenic defects found correlate with alterations of the segmentation clock, we analyzed the expression of *Hes5* and *Lnfg* – factors involved in cyclic expression in the presomitic mesoderm; however, we did not find any alterations in the expression of the mRNAs for these factors (Fig. S7).

A positive-feedback loop maintains the retinoic acid pathway and Meis gene expression during axial patterning

In the transcriptomic analysis of *Meis* mutants, *Raldh2* – the gene encoding the main enzyme responsible for embryonic RA synthesis – and *Cyp26b1* – the gene encoding the main enzyme responsible for RA degradation in the embryo – appeared to be downregulated in the anterior trunk region by RNA-seq (Fig. S6). *In situ* hybridizations for both genes were consistent with the transcriptomic analysis. *Raldh2* expression appeared reduced at E9.5 in the differentiating derivatives of anterior somites but not in the presomitic area or in newly produced somites (Fig. 6A-B″). A similar pattern is present at E10.5, where tail regions with newly produced somites do not show alterations, but more anterior regions do show a reduction in *Raldh2* transcripts (Fig. 6C-D″).

In the somitic region of E9 embryos, *Cyp26b1* is expressed exclusively in the endothelium of the dorsal aortae and inter-somitic vessels, whereas it is strongly expressed in areas of the hindbrain. The hindbrain signal was preserved in mutants; however, the endothelial signal in the trunk region was lost (Fig. 6E-F′). *Cyp26b1* is a direct target of the RA pathway that is activated in response to

Development (2021) 148, dev193813. doi:10.1242/dev.193813

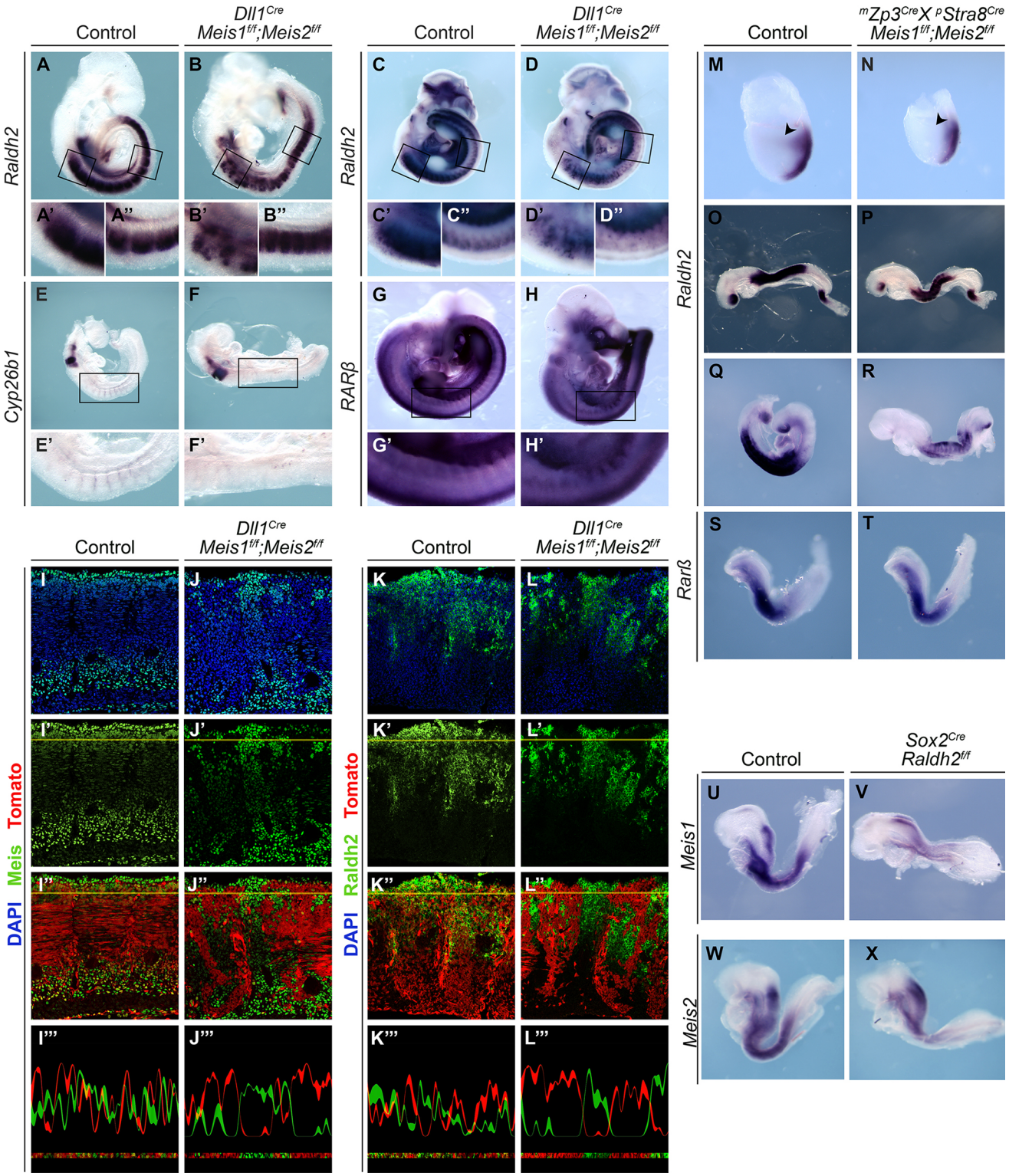

Fig. 6. Cross-regulatory interactions between Meis and the retinoic acid pathway. (A-D″) *Raldh2* mRNA *in situ* hybridization in E9.5 (A-B″) and E10.5 (C-D″) Meis mutant embryos. (E-F′) *Cyp26b1* mRNA *in situ* hybridization in E9 Meis mutant embryos. (G-H′) *Rarb* mRNA *in situ* hybridization in E10.5 Meis mutant embryos. (A′-H′,A″-D″) Magnification of the regions marked in the upper images. (I-L″) *Dll1*^{Cre} recombination pattern reported by a *Rosa26R*^{tdTomato} allele in the anterior somites of E10.5 embryos. MEIS and RALDH2 immunofluorescence (I-L″), and corresponding quantification plots (I‴-L‴) along the indicated yellow lines in I′-L″. (M-R) *Raldh2* mRNA *in situ* hybridization in embryos at E7.5 (M,N), E8.75 (O,P) and E9 (Q,R) of control (M,O,Q) and maternally and paternally recombined *Meis1*$^{f/f}$;*Meis2*$^{f/f}$ (N,P,R) embryos. Arrowheads indicate the *Raldh2* expression domain in the lateral plate in M and its absence in N. (S,T) *Rarb* mRNA *in situ* hybridization in E8.5 maternally and paternally recombined *Meis1*$^{f/f}$;*Meis2*$^{f/f}$ embryos (T) and their controls (S). (U-X) *Meis1* and *Meis2* mRNA *in situ* hybridization in control (U,W) and *Sox2*^{Cre};*Raldh2*$^{f/f}$ (V,X) E8.5 embryos. ^{m}*Zp3*^{Cre} indicates maternal presence of the allele and ^{p}*Stra8*^{Cre} indicates paternal presence of the allele.

Development (2021) 148, dev193813. doi:10.1242/dev.193813

RA. The concomitant downregulation of *Raldh2* and *Cyp26b1* thus suggest that Meis mutant embryos have defective RA. We then studied the expression of the gene encoding the RA β receptor (*Rarb*), which has been described as a RA-responsive gene. Contrary to expectations, no change in the pattern of *Rarb* mRNA was detected between controls and Meis mutants (Fig. 6G-H′), which is consistent with the RNAseq analysis, which identified no differences in *Rara*, *Rarb* or *Rarg*. The observations on the expression levels of *Raldh2*, *Cyp26b1* and *Rarb* mRNAs were also confirmed by quantitative PCR (Fig. S8).

Unexpectedly, several of the embryos studied showed *Raldh2* reduction in a mosaic fashion. To understand why the reductions in *Raldh2* appeared mosaic, we combined $Meis1^{flox}$ and $Meis2^{flox}$ alleles with $Dll1^{Cre}$ and a $Rosa26R^{tdTomato}$ reporter. In these embryos, $Dll1^{Cre}$ recombines the $Rosa26R^{tdTomato}$ reporter, allowing the Cre recombination pattern to be determined. At E10.5, E9.5 and E8.5, we observed a mosaic pattern of Tomato$^+$ cell distribution in both control and Meis mutant embryos, with variability in the proportion of Tomato$^+$ cells found in the somites of different embryos (Fig. S9). This mosaicism had not been described for this line before (Wehn et al., 2009), and therefore it might depend on the genetic background. To determine whether the observed mosaicism results from inefficient recombination in all cells or from mosaic activation of $Dll1^{Cre}$ expression, we studied the correlation between Meis immunodetection and Tomato expression in $Dll1^{Cre}$;$Rosa26R^{tdTomato}$;$Meis1^{flox/flox}$;$Meis2^{flox/flox}$ embryos. We found that Tomato$^+$ cells were devoid of Meis, whereas their neighboring Tomato$^-$ cells showed Meis expression (Fig. 6I-J‴). Image profiling shows anti-correlation between Tomato and Meis detection in mutants (Fig. 6J‴), whereas this was not found in control embryos (Fig. 6I‴). These observations indicate that the pattern observed results from mosaic inactivation of $Dll1^{Cre}$ and therefore the Tomato$^+$ cell distribution reports the distribution of Meis-deficient cells. In mutants, we found a tendency of knockout and wild-type cells to segregate from each other, resulting in large aggregates of Tomato$^+$ cells that were not found in controls (Fig. 6I″,J″). We did not find any reproducible difference between mutant and control embryos in the distribution of Tomato$^+$ cell patches by tissues. In addition, the anterior-most border of Tomato$^+$ cell distribution was established at the occipital level and this did not differ between control and mutant embryos.

We therefore used the mosaic inactivation of Meis alleles to study the regulation of *Raldh2* by MEIS. We performed Raldh2 immunostaining and correlated this signal with that of Tomato. We found that Tomato$^+$ cells lacking MEIS function did not present detectable RALDH2 expression, while their Tomato$^-$, Meis-expressing neighboring cells showed normal Raldh2 expression (Fig. 6K-L‴). The result was similar to that observed for MEIS immunostaining, with the signals for RALDH2 and Tomato being mutually exclusive in mutant embryos but not in controls (Fig. 6K″,L″). These results indicate a strict and cell-autonomous requirement for Meis function in *Raldh2* expression in the differentiating trunk mesoderm.

We then analyzed *Raldh2* expression in embryos with double maternal/zygotic inactivation of *Meis1* and *Meis2* (Fig. 6M-R). *Raldh2* mRNA distribution in the early embryo resembles *Meis* expression pattern; however, it starts slightly later and affects only the mesoderm (Fig. S10). In mutant embryos, we observed no alteration of the expression pattern in the axial and paraxial mesoderm; however, the lateral plate domain close to the extra-embryonic region was abolished (arrowheads in Fig. 6M,N). Up to E8.75, no alteration of *Raldh2* expression in the paraxial mesoderm was observed (Fig. 6O,P); however, at E9, all trunk *Raldh2* expression was strongly decreased in mutants (Fig. 6Q,R). The reduction in *Raldh2* and *Cyp26b1* was confirmed by qPCR in four out of five embryos with complete absence of *Meis1* and *Meis2* (Fig. S8); however, no reduction was observable for *Rarb* by either RNA *in situ* hybridization or qRT-PCR (Fig. 6G-H′,S,T; Fig. S8). Although RALDH2 is the main enzyme for RA synthesis in the embryo, RALDH3 is also present in embryos and contributes to RA generation. To determine whether *Raldh3* activation could contribute to RA synthesis, we studied transcript abundance by qRT-PCR and found instead reduced expression in three out of six embryos in the *Dll1Cre* model and in all five embryos with complete absence of *Meis1* and *Meis2* (Fig. S8). These results show that Meis controls RA synthesis by maintaining transcription of genes encoding essential RA-synthesizing enzymes. Contrary to expectations, this does not result in reduced transcription of the RA direct target *Rarb*.

Given that retinoic acid has been shown to regulate Meis expression in different settings (Berenguer et al., 2020; Mercader et al., 2000; Oulad-Abdelghani et al., 1997; Yashiro et al., 2004), we studied whether the elimination of *Raldh2*-mediated RA synthesis affects axial Meis expression. We studied *Meis1* and *Meis2* mRNA expression in $Sox2^{Cre}$;$Raldh2^{flox/flox}$ embryos, and found that both genes presented lower levels of transcripts along the trunk region of E8 embryos (Fig. 6U-X).

These results indicate that Meis is required for maintenance of *Raldh2* expression in the differentiating paraxial mesoderm but not for its initial expression before somite differentiation. These conclusions correlate with the observed downregulation of *Raldh2*/*Cyp26b1* in the transcriptome of the anterior trunk but not the posterior trunk of E9.5 embryos. In contrast, the early lateral plate mesoderm – likely fated to the cardiogenic area – requires Meis activity for *Raldh2* expression from the earliest stages. Reciprocally, *Raldh2* expression is required to maintain proper *Meis* expression levels, but not for initiating *Meis* expression, given that *Meis* expression starts before *Raldh2* expression. These results indicate that there is a positive regulatory loop between *Meis* and *Raldh2* that is relevant to mutually maintain but not initiate their expression.

Raldh2 deficiency produces axial skeleton defects partially overlapping with those observed in Meis mutants

Although retinoic acid has long been postulated as a regulator of axial skeleton, there is no direct study of the consequences of eliminating RA on anterior-posterior axial identities. Here, we conditionally deleted *Raldh2* using $Dll1^{Cre}$ to investigate whether this affects the axial skeleton and the extent to which RA might be related to Meis roles in axial patterning. In the occipital region, the basioccipital presented similar alterations to those observed in Meis mutants (n=14/43) (Fig. 7A,F; Table S1D,E), including its fusion with the aaa (arrowhead in Fig. 7F). Strikingly, similar modifications of the basioccipital were also found in some control embryos, although in a lower proportion (n=5/47) (Fig. 7F,P), suggesting a genetic background prone to these particular defects. In mutants, C1 appeared fused to, and/or adopting a shape and position similar to, the exoccipital (n=8/49) (Fig. 7H,P; Fig. S11). In the cases in which C1 showed transformation to exoccipital, C2 adopted a C1 morphology (n=8/41), whereas some cases in which C1 retained its morphology, C2 adopted a C1 morphology and partially fused to C1 (n=9/41) (Fig. 7H,P; Fig. S11). C3 to C2 transformations/fusions were also observed (n=11/41) (Fig. 7P). At the cervical thoracic transition, tuberculi anterior were found in C7 instead of C6 (n=5/21) (Fig. 7C,H, arrow in 7H; Fig. S11), suggesting that anterior transformations also take place at this axial

Development (2021) 148, dev193813. doi:10.1242/dev.193813

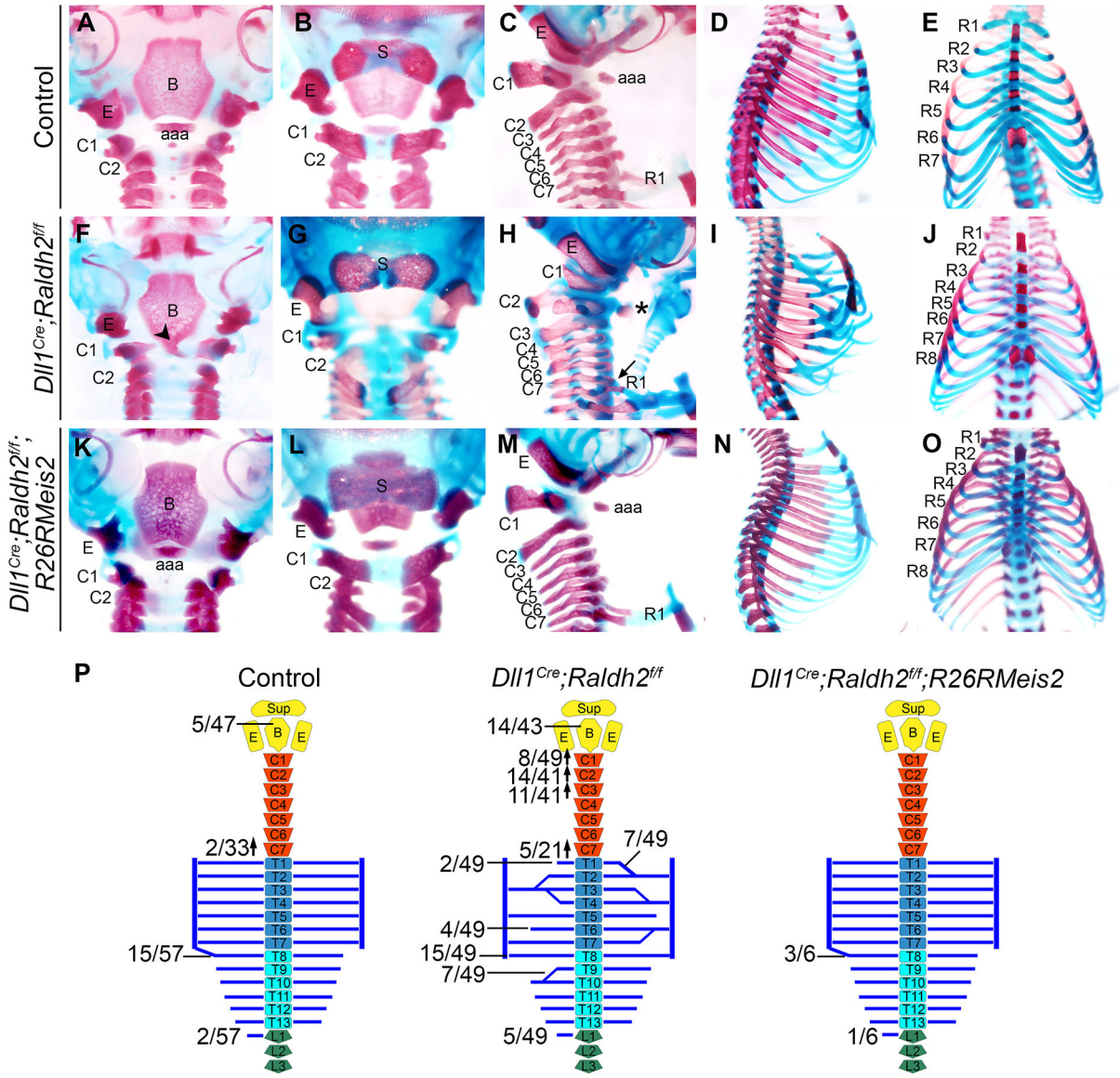

Fig. 7. Skeletal defects in *Dll1^{Cre};Raldh2$^{f/f}$* fetuses and their rescue by Meis2 expression. (A-O) Skeletal staining of E18.5 fetuses of the indicated genotypes. (A,F,K) Ventral view of the basioccipital. Arrowhead in F indicates fusion between basioccipital and aaa. (B,G,L) Dorsal view of the supraoccipital. (C,H,M) Cervical region. In H, asterisk indicates aaa formed by C2 and arrow indicates tuberculi anterior in C7. (D,I,N) Thoracic region. (E,J,O) Ventral view of the sternum. (P) Schematic representation of the axial skeletal defects observed and their frequencies. Upward and downward arrows, respectively, indicate anterior or posterior homeotic transformations. aaa, anterior arch of the atlas; B, basioccipital; C, cervical vertebra; E, exoccipital; R, rib; S, supraoccipital.

level. Altogether, the alterations found in *Raldh2* mutants in the occipital/cervical regions were similar to those observed in Meis mutants but displayed lower penetrance (Fig. 7P).

In the thoracic region, shortening or fusion of the first rib with the second rib and generalized rib fusions and bifurcations were observed, similar to the defects found in Meis mutants (Fig. 7D,I). In the most affected mutant embryos, we observed defects in the inter-sternal cartilage and the sternebrae, although we did not observe a split sternum (Fig. 7E,J). Some incidences of an extra sternal rib and an extra rib on L1 were also observed (Fig. 7E,J,P), suggesting AP transformations were extensive down to the thoracic/lumbar transition.

The compared analysis of Meis and *Raldh2* mutants supports the idea that MEIS and the retinoic acid pathway act in a positive-feedback loop that is relevant in patterning the axial skeleton. To obtain evidence for the functional relevance of this regulatory loop and determine its relevant output in axial patterning, we used a *Rosa26R$^{Meis2\text{-}EYFP}$* allele (Rosello-Diez et al., 2014) that provides *Meis2* overexpression coupled to *IRES-EYFP* expression upon Cre recombination. We then simultaneously eliminated *Raldh2* and activated *Meis2* with *Dll1^{Cre}*. Co-staining for detection of GFP and RALDH2 confirmed deletion of *Raldh2* concomitant with *Meis2* activation (Fig. S12). Interestingly, in this mouse model, all defects produced by *Raldh2* mutation in the axial skeleton were rescued (Fig. 7K-P; Table S1D,E), indicating that Meis suppresses the effect of RA deficiency on axial skeleton patterning.

DISCUSSION

Although *Meis1* and *Meis2* expression starts at gastrulation, their early patterns are different in time and expression domains. *Meis2* is activated earlier than *Meis1* in a pattern that coincides spatially and temporally with that of Hox gene activation in the posterior epiblast.

Development (2021) 148, dev193813. doi:10.1242/dev.193813

We have not observed major alterations in Hox gene expression patterns or transcript abundance in *Meis* mutants. These results indicate that, despite the profuse binding of Meis proteins to the Hox complexes (Penkov et al., 2013), Meis is not essential for Hox gene transcriptional regulation during axial skeleton patterning. This does not apply to other embryonic regions, given that we have observed clear alterations of Hox mRNA expression domains in limb buds with altered Meis function (Delgado et al., 2020; Mercader et al., 1999, 2009; Rosello-Diez et al., 2014) and similar results have been reported during neural patterning in other vertebrate species (Dibner et al., 2001; Vlachakis et al., 2001; Waskiewicz et al., 2001) and are reported here in the mouse (Fig. 4). The observed binding of MEIS to the Hox complexes might therefore be involved in regulating Hox transcription in several tissues but not in the paraxial mesoderm, at least at the stages studied here.

Despite the absence of changes in Hox transcription in the paraxial mesoderm, Meis mutants produce anterior homeotic transformations and defects similar to those previously described for Hox mutants affecting the occipital and cervical regions (Horan et al., 1995; Jeannotte et al., 1993; Manley and Capecchi, 1997; McIntyre et al., 2007). This is consistent with studies in flies in which the elimination of the Meis ortholog *homothorax* produces homeotic phenotypes by modifying the DNA affinity and target selectivity of HOX proteins without altering Hox gene transcription (Merabet and Mann, 2016; Rieckhof et al., 1997). We thus propose that, during axial patterning in vertebrates, Meis regulates Hox function by directly binding HOX proteins and regulating their affinity and selectivity for target DNA sequences, through their described HOX-co-factor activity.

We deleted *Meis2* using Cre lines that recombine at different stages of epiblast cell recruitment to the paraxial mesoderm; however, we did not find any substantial influence of the timing of *Meis2* removal on the phenotypes obtained. The early expression of *Meis2* in the posterior epiblast thus seems not to play any role in axial skeletal patterning, whereas both *Meis1* and *Meis2* cooperate in the presomitic mesoderm, or at later stages of somite development, in axial patterning.

Apart from its function in segmental identity, the transcriptional analysis of the mutants indicates an important function in hypaxial myotome development, with profound alterations of the myogenic pathways and phenotypes that have not been reported in Hox mutants. Interestingly, *Myf5*, *Mrf4* and myogenin-deficient mice show rib defects similar to those described here (Braun et al., 1992; Hasty et al., 1993; Patapoutian et al., 1995), and, therefore, the failure in proper activation of the hypaxial myogenic program is sufficient to explain rib mispatterning in *Meis1/Meis2* DKOs. Moreover, hypaxial myotomal *Fgf4* and *Fgf6* expression, which is required for rib patterning downstream of the myogenic factors (Vinagre et al., 2010), is strongly impaired in Meis mutants, indicating a function of MEIS in the crosstalk between myotome and sclerotome. In addition, the activation of the myogenic program involved in rib pattering is under direct control of a specific set of HOX proteins involved in the specification of thoracic segments (Vinagre et al., 2010). The rib mispatterning phenotypes may therefore also partly involve the impairment of Hox function in the absence of MEIS.

RNA-seq analysis, quantitative PCR and/or *in situ* hybridization revealed a reduction in *Raldh2*, *Raldh3* and *Cyp26b1* in Meis mutants. RALDH enzymes are essential for RA synthesis and, therefore, Meis mutant embryos presumably contain reduced levels of RA. As the activation of *Cyp26b1* is RA dependent, its downregulation in Meis mutants could be a secondary event, due to the reduction in RA synthesis by RALDH2. A contradictory result is the observation that *Rarb*, a well described target of RA, does not show reduced expression in Meis-deficient embryos. We do not have a clear explanation for this result; it could indicate a lower RA threshold for *Rarb* activation than for *Cyp26b1* activation or a more complex situation in which its transcriptional dependence on RA is modified by the absence of Meis.

Cyp26b1 mutants show posterior homeotic transformations in the occipital/cervical region associated with increased RA levels (Sakai et al., 2001). The posterior transformations in this model are the opposite of those observed in Meis mutants, which concurs with the idea that Meis is a positive regulator of RA synthesis. In addition, *in vivo* treatments with RA during mouse gestation caused either anterior or posterior homeotic transformations, depending on the stage of the treatment (Kessel and Gruss, 1991). In the cervical region, anterior transformations were observed following treatments at E7, while posterior transformations were found following RA treatment from E8 (Kessel, 1992). Here, we generated a *Raldh2* conditional knockout using the *Dll1*^{Cre} driver and found homeotic transformations affecting the occipital/cervical region, and additional patterning defects in the thoracic region that significantly overlap with those observed in Meis mutants. In agreement with this, mutations in retinoic acid receptor genes produce homeotic transformations (Lohnes et al., 1993, 1994), similar to those observed in Meis mutants. In particular, *Rarg* and *Rarb* loss-of-function mutants show anterior transformations without showing any changes in Hox expression patterns (Folberg et al., 1999a,b).

We described a positive regulatory loop between MEIS and RALDH2 that we confirmed using functional genetic analysis. The similarities in skeletal transformations between *Raldh2* and Meis mutants and the cross-regulation between *Raldh2* and Meis suggest that the positive regulatory loop between *Raldh2* and Meis is involved in axial patterning. Although Meis genes are RA targets in various contexts (Mercader et al., 2000; Oulad-Abdelghani et al., 1997; Yashiro et al., 2004), *Raldh2* is a direct Meis target in the hindbrain (Vitobello et al., 2011), and ChIPseq analysis in E10.5 limb buds identifies MEIS-binding sites in the *Raldh2* locus (Delgado et al., 2020). In fact, MEIS could promote RA accumulation at various levels, as it also represses *Cyp26b1* during limb development in a cell-autonomous manner (Rosello-Diez et al., 2014). The requirement of Meis activity for *Raldh2* transcription in the paraxial mesoderm is restricted to the differentiation stages and does not take place in the nascent or segmenting mesoderm. In concurrence with our findings, *Pbx1/Pbx2*-null embryos show normal *Raldh2* expression at early embryonic stages, but strong downregulation in the paraxial mesoderm at E9.0 and beyond (Vitobello et al., 2011). Finally, we studied the functional output of the MEIS-RA regulatory loop by genetic rescue. The complete rescue of *Raldh2* mutants by Meis overexpression suggest that MEIS is the main functional output of the positive regulatory loop between Meis and RA in the paraxial mesoderm.

We propose a model for the RA-Meis-Hox network in the paraxial mesoderm in which Meis is involved in a positive-feedback loop with RA through *Raldh2* regulation (Fig. 8). Meis is the main output of this regulatory loop and is required for the specification of axial skeletal identities, likely through regulating HOX protein activity. The proposed model would explain the ability of RA and RARs to phenocopy Hox mutants without affecting their transcriptional expression. In addition, as deduced from the segmentation and myogenic phenotypes, Meis factors play roles unrelated to Hox function.

Development (2021) 148, dev193813. doi:10.1242/dev.193813

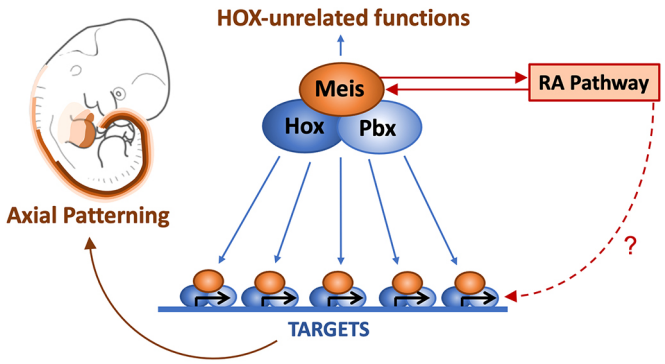

Fig. 8. Model for the regulatory interactions between retinoic acid, MEIS, PBX and HOX factors. Meis controls the function of Hox proteins in cooperation with Pbx during axial skeleton patterning. The retinoic acid (RA) pathway can affect Hox activity through regulating Meis levels in a positive feedback loop. The RA-Meis regulatory loop affects additional Hox-independent functions, whereas direct activity of the RA pathway on Hox transcription cannot be excluded.

MATERIALS AND METHODS

Mouse lines and embryo harvest

Experiments were performed using mice (*Mus musculus*). Mice were handled in accordance with CNIC Ethics Committee, Spanish laws and the EU Directive 2010/63/EU for the use of animals in research. All mouse experiments were approved by the CNIC and Universidad Autónoma de Madrid Committees for 'Ética y Bienestar Animal' and the area of 'Protección Animal' of the Community of Madrid with reference PROEX 220/15.

Meis conditional knockouts were generated mating *Meis1*^{flox} (Unnisa et al., 2012) and *Meis2*^{flox} (Delgado et al., 2020) with different Cre lines: *Sox2*^{Cre} (Hayashi et al., 2002), *Mesp1*^{Cre} (Saga et al., 1999), *Dll1*^{Cre} (Wehn et al., 2009), *Stra8*^{Cre} (Sadate-Ngatchou et al., 2008) and *Zp3*^{Cre} (de Vries et al., 2000). *Raldh2* conditional knockouts were obtained by mating *Raldh2*^{flox} mice (Vermot et al., 2006) with *Dll1*^{Cre} and *Sox2*^{Cre}. For Cre^{+} cell-lineage tracing, we used *Gt(ROSA)*$^{26Sortm14(CAG-tdTomato)Hze}$ (Madisen et al., 2010). For conditional Meis overexpression we used the *Rosa26R*$^{Meis2-EYFP}$ line (Rosello-Diez et al., 2014).

To obtain embryos at different gestational stages, mice were mated in the afternoon and females were checked every morning for the presence of a vaginal plug; noon on the day the plug was observed was considered as gestational day 0.5 (E0.5). Embryos at somitogenic stages were staged according to age and somite number. Embryos that had not started somitogenesis were staged according to Downs and Davies (1993).

In situ hybridization

Embryos were fixed in 4% PFA overnight at 4°C. Embryos were dehydrated and rehydrated washing them with increasing and decreasing, respectively, concentrations of methanol in PBT (25%, 50%, 75% and 100%). Bleaching was carried out by incubation in 6% H_2O_2 in PBT for 1 h. Proteinase K (Sigma) digestion was performed at 10 µg/ml with different incubation times depending on the stage. After permeabilization, embryos were washed with PBT for 5 min and fixed with 0.05% glutaraldehyde in 4% PFA for 20 min. Embryos were incubated in hybridization buffer [50% formamide, 4× SSC (pH 4.5), 1% SDS, 50 µg/ml heparin (Sigma), 10 µg/ml tRNA from baker's yeast (Sigma) and 1% w/v Blocking reagent (Sigma)] for 2 h and hybridized with the probe overnight at 65°C. Post-hybridization washes were performed with 0.1% w/v CHAPS (Sigma) and 2× SSC (pH 5.5), followed by a second round of post-hybridization washes with 0.1% w/v CHAPS and 0.2× SSC for 3 h at 65°C. Embryos were incubated overnight at 4°C with 1:2000 anti-digoxigenin AP antibody (Roche) in 20% goat serum, 1% blocking reagent in TBST [5 mM Tris-HCl (pH 7.5), 15 mM NaCl and 0.1% Triton X-100 (Sigma)]. After several washes in TBST, embryos were washed with 125 mM Tris-HCl (pH 9.5), 125 mM NaCl, 62.5 mM $MgCl_2$ and 0.5% Triton X-100, and stained with BMPurple (Roche) at room temperature until the signal was optimal. After the staining, embryos were washed with TBST, fixed in 4% PFA and stored at 4°C. Occasionally, after *in situ* hybridization, embryos were gelatin embedded and cryosectioned.

Probe synthesis

RNA antisense probes were synthesized by transcription of linearized DNA from plasmids or from cDNA amplified with specific primers (Table S2). Transcription was carried out with digoxigenin-labeled nucleotides (Roche) and T7 RNA polymerase (Roche). Synthesized RNA was precipitated with 0.8 M ammonium acetate in 75% ethanol or 0.1 M LiCl in 75% ethanol and finally resuspended in 50% formamide-50% RNase free water.

Victoria Blue staining

Embryos at E14.5 were eviscerated and fixed in 10% formaldehyde overnight and then washed in acid alcohol (3% HCl in 70% ethanol) several times. Embryos were stained for 3 h with 0.5% w/v Victoria Blue (Sigma) in acid alcohol and after staining embryos were washed in acid alcohol until the embryos were white, then they were washed in 70% ethanol and 95% ethanol. Finally, embryos were clarified with increasing concentrations of methyl salicylate in ethanol (30% and 50%) and stored in 100% methyl salicylate.

Alcian Blue and Alizarin Red staining

Embryos at E18.5 were eviscerated and the skin and soft tissues were removed as much as possible. Embryos were fixed overnight with 95% ethanol and after fixation were submerged in Alcian Blue solution [0.03% w/v Alcian Blue (Sigma), 80% ethanol and 20% glacial acetic acid] overnight. Alcian Blue solution was removed and several washes with 70% ethanol were made during the day with incubation in 95% ethanol overnight. Once the tissue becomes whiter, embryos were cleared with 1% KOH for 3-6 h depending on the stage and the amount of soft tissue that the embryos had. Once cleared, Alizarin Red solution [0.005% Alizarin Red (Sigma) and 1% w/v KOH] was added until the bones were stained. Another clarification step with 1% KOH could be carried out if necessary after staining with Alizarin Red solution, otherwise embryos were transferred to increasing concentrations of glycerol (20% and 50%) and finally placed in 100% glycerol for long-term storage.

Immunostaining and imaging

Embryos were fixed in 2% PFA, gelatin embedded and cryosectioned. Sections were permeabilized with 0.5% Triton X-100 in PBS for 20 min and blocking was performed with 20% goat serum in PBS for 1 h. The primary antibodies used overnight at 4°C were anti-GFP (Aves laboratories, GFP-1020, 1:200) rabbit anti-RALDH2 (Abcam, ab96060, 1:200) and an anti-MEISa, recognizing C-terminal short isoform of MEIS1 and MEIS2 (Mercader et al., 2005). Secondary antibodies were incubated for 45 min at room temperature. Secondary antibodies used were Alexa-488 (Life Technologies, A11034, 1:500) for anti-MEISa and anti-RALDH2; anti-rabbit-HRP (Dako, P0448, 1:200) for anti-RALDH2 and anti-chicken Alexa-594 (Abcam, ab15172, 1:500) for anti-GFP. Following anti-rabbit-HRP incubation, amplification with Tyr-FITC (Perkin Elmer, NEL74100KT, 1:100) for 3 min at room temperature was performed. Sections were incubated with DAPI and mounted in Vectashield or Dako fluorescent mounting media for acquisition. Images were acquired using a Nikon A1R confocal microscope using 405, 488 and 561 nm wavelengths and Plan Apo 10× DIC L or Plan Apo VC 20× DIC N2 dry objectives.

Quantitative PCR

E9 embryos were eviscerated and the embryonic tissue posterior to the otic vesicle, containing the paraxial mesoderm and the neural tube, was selected and frozen. RNA purification was carried out using the Qiagen miRNeasy Mini Kit and retrotranscribed using Invitrogen SuperScript II Reverse Transcriptase. qPCR was then performed using Sybr Green PCR Master Mix and run in an ABI Prism 7000 from Applied Biosystems. Primers used were as follows: *Raldh2* (forward), GAAGGATGGATGCGTCTGAAA; *Raldh2* (reverse), TTCCACCAAGTCTGCAAGCTT; *Rarb* (forward), TATGAGATGACAGCGGAGCTAGAC; *Rarb* (reverse), GGCTTTCCG-GATCTTCTCAGT; *Cyp26b1* (forward), AATGAGATTCTGCCGGAG-ACA; *Cyp26b1* (reverse), GAGGCTACACCGTAGCACTCAA; *Raldh3*

Development (2021) 148, dev193813. doi:10.1242/dev.193813

(forward), AGAGTGCGAACCAGTTATGGC; *Raldh3* (reverse), ATCTCCTTCTTCCACCTCACATA.

mRNA sequencing

Differential gene expression analysis was carried out between $Dll1^{Cre}$;$Meis1^{flox/flox}$;$Meis2^{flox/flox}$ and control embryos at E9. Four embryos were used for each condition and were staged by somite number, choosing the embryos with 20-24 somites. Total RNA was isolated using RNeasy Micro Kit (Qiagen) separating the anterior region, containing the first 10-12 somites (the head was excluded), from the posterior region, with the rest of the somites and the posterior embryonic bud. Total RNA (20 ng) was used to generate barcoded RNA-seq libraries using the NEBNext Ultra RNA Library preparation kit (New England Biolabs). The size and the concentration of the libraries were checked using the TapeStation 2200 DNA 1000 chip. Libraries were sequenced on a HiSeq2500 (Illumina) to generate 60-base single reads. FastQ files for each sample were obtained using bcltofastQ software 2.20.

RNA-seq data analysis

Sequencing reads were pre-processed by means of a pipeline that used FastQC (http://www.bioinformatics.babraham.ac.uk/projects/fastqc/) to assess read quality, and Cutadapt (Martin, 2011) to trim sequencing reads (eliminating Illumina adaptor remains) and to discard reads that were shorter than 30 bp. The resulting reads were mapped against the mouse transcriptome (GRCm38, release 91; dec2017 archive) and quantified using RSEM v1.2.20 (Li and Dewey, 2011). Data were then processed with a pipeline that used Bioconductor package Limma (Ritchie et al., 2015) for normalization and differential expression analysis, using a blocking strategy to consider gender and developmental stage (number of somites). Genes with at least one count per million in at least four samples (14,731 genes) were considered for further analysis. We considered as differentially expressed those genes with Benjamini-Hochberg adjusted P value <0.05. Fold change and log(ratio) values were calculated to represent gene expression differences between conditions. Ingenuity Pathway Analysis software from Qiagen was used to identify regulatory pathway enrichment.

Acknowledgements

We thank members of the Torres group for stimulating discussions and suggestions. We thank members of the Genomics, Bioinformatics, Pluripotent Cell Technology, Transgenesis and Animal Facility CNIC units for excellent support. *Meis1* floxed mice were generated by Keith Humphries and kindly provided by Hesham Sadek. We thank Miguel Manzanares for providing mouse strains, and Marian Ros, Aimee Zuniga, Paola Bovolenta, Robb Krumlauf and Jose Luis de la Pompa for kindly providing *in situ* probes.

Competing interests

The authors declare no competing or financial interests.

Author contributions

Conceptualization: A.C.L.-D., M.T.; Methodology: A.C.L.-D., I.D., V.C., F.S.-C.; Formal analysis: A.C.L.-D., F.S.-C.; Investigation: A.C.L.-D., I.D., M.T.; Writing - original draft: A.C.L.-D., M.T.; Writing - review & editing: A.C.L.-D., I.D., M.T.; Supervision: M.T.; Funding acquisition: M.T.

Funding

This research was supported by the Ministerio de Ciencia, Innovación y Universidades (PGC2018-096486-B-I00), the Instituto de Salud Carlos III (RD16/0011/0019) and by the Comunidad de Madrid (S2017/BMD3875). The Centro Nacional de Investigaciones Cardiovasculares Carlos III is supported by the Ministerio de Ciencia, Innovación y Universidades and the Pro Centro Nacional de Investigaciones Cardiovasculares Carlos III Foundation, and is a Severo Ochoa Center of Excellence (SEV-2015-0505). A.C.L.-D. was the recipient of a Formación Personal Investigador fellowship from the Ministerio de Economía y Competitividad (BES-2013-064374).

Data availability

The RNA-seq data have been deposited in GEO under accession number GSE146301.

Supplementary information

Supplementary information available online at
https://dev.biologists.org/lookup/doi/10.1242/dev.193813.supplemental

Peer review history

The peer review history is available online at
https://dev.biologists.org/lookup/doi/10.1242/dev.193813.reviewer-comments.pdf

References

Alexander, T., Nolte, C. and Krumlauf, R. (2009). Hox genes and segmentation of the hindbrain and axial skeleton. *Annu. Rev. Cell Dev. Biol.* **25**, 431-456. doi:10.1146/annurev.cellbio.042308.113423

Amin, S., Donaldson, I. J., Zannino, D. A., Hensman, J., Rattray, M., Losa, M., Spitz, F., Ladam, F., Sagerström, C. and Bobola, N. (2015). Hoxa2 selectively enhances Meis binding to change a branchial arch ground state. *Dev. Cell* **32**, 265-277. doi:10.1016/j.devcel.2014.12.024

Berenguer, M., Meyer, K. F., Yin, J. and Duester, G. (2020). Discovery of genes required for body axis and limb formation by global identification of retinoic acid-regulated epigenetic marks. *PLoS Biol.* **18**, e3000719. doi:10.1371/journal.pbio.3000719

Braun, T., Rudnicki, M. A., Arnold, H.-H. and Jaenisch, R. (1992). Targeted inactivation of the muscle regulatory gene Myf-5 results in abnormal rib development and perinatal death. *Cell* **71**, 369-382. doi:10.1016/0092-8674(92)90507-9

Capellini, T. D., Zewdu, R., Di Giacomo, G., Asciutti, S., Kugler, J. E., Di Gregorio, A. and Selleri, L. (2008). Pbx1/Pbx2 govern axial skeletal development by controlling Polycomb and Hox in mesoderm and Pax1/Pax9 in sclerotome. *Dev. Biol.* **321**, 500-514. doi:10.1016/j.ydbio.2008.04.005

Chan, S.-K., Jaffe, L., Capovilla, M., Botas, J. and Mann, R. S. (1994). The DNA binding specificity of Ultrabithorax is modulated by cooperative interactions with extradenticle, another homeoprotein. *Cell* **78**, 603-615. doi:10.1016/0092-8674(94)90525-8

Chang, C. P., Brocchieri, L., Shen, W. F., Largman, C. and Cleary, M. L. (1996). Pbx modulation of Hox homeodomain amino-terminal arms establishes different DNA-binding specificities across the Hox locus. *Mol. Cell. Biol.* **16**, 1734-1745. doi:10.1128/MCB.16.4.1734

Choe, S.-K., Ladam, F. and Sagerström, C. G. (2014). TALE factors poise promoters for activation by Hox proteins. *Dev. Cell* **28**, 203-211. doi:10.1016/j.devcel.2013.12.011

de Vries, W. N., Binns, L. T., Fancher, K. S., Dean, J., Moore, R., Kemler, R. and Knowles, B. B. (2000). Expression of Cre recombinase in mouse oocytes: a means to study maternal effect genes. *Genesis* **26**, 110-112. doi:10.1002/(SICI)1526-968X(200002)26:2<110::AID-GENE2>3.0.CO;2-8

Delgado, I., López-Delgado, A. C., Roselló-Díez, A., Giovinazzo, G., Cadenas, V., Fernández-del-Manuel, L., Sánchez-Cabo, F., Anderson, M. J., Lewandoski, M. and Torres, M. (2020). Proximo-distal positional information encoded by an Fgf-regulated gradient of homeodomain transcription factors in the vertebrate limb. *Sci. Adv.* **6**, eaaz0742. doi:10.1126/sciadv.aaz0742

Deschamps, J. and Duboule, D. (2017). Embryonic timing, axial stem cells, chromatin dynamics, and the Hox clock. *Genes Dev.* **31**, 1406-1416. doi:10.1101/gad.303123.117

Deschamps, J., de Laaf, R., Joosen, L., Meijlink, F. and Destree, O. (1987). Abundant expression of homeobox genes in mouse embryonal carcinoma cells correlates with chemically induced differentiation. *Proc. Natl. Acad. Sci. USA* **84**, 1304-1308. doi:10.1073/pnas.84.5.1304

Deschamps, J., van den Akker, E., Forlani, S., De Graaff, W., Oosterveen, T., Roelen, B. and Roelfsema, J. (1999). Initiation, establishment and maintenance of Hox gene expression patterns in the mouse. *Int. J. Dev. Biol.* **43**, 635-650.

Dibner, C., Elias, S. and Frank, D. (2001). XMeis3 protein activity is required for proper hindbrain patterning in Xenopus laevis embryos. *Development* **128**, 3415-3426.

Downs, K. M. and Davies, T. (1993). Staging of gastrulating mouse embryos by morphological landmarks in the dissecting microscope. *Development* **118**, 1255-1266.

Duboule, D. and Dollé, P. (1989). The structural and functional organization of the murine HOX gene family resembles that of Drosophila homeotic genes. *EMBO J.* **8**, 1497-1505. doi:10.1002/j.1460-2075.1989.tb03534.x

Folberg, A., Kovács, E. N., Huang, H., Houle, M., Lohnes, D. and Featherstone, M. S. (1999a). Hoxd4 and Rarg interact synergistically in the specification of the cervical vertebrae. *Mech. Dev.* **89**, 65-74. doi:10.1016/S0925-4773(99)00203-8

Folberg, A., Nagy Kovács, E., Luo, J., Giguère, V. and Featherstone, M. S. (1999b). RARβ mediates the response of Hoxd4 and Hoxb4 to exogenous retinoic acid. *Dev. Dyn.* **215**, 96-107. doi:10.1002/(SICI)1097-0177(199906)215:2<96::AID-DVDY2>3.0.CO;2-T

Grass, S., Arnold, H. H. and Braun, T. (1996). Alterations in somite patterning of Myf-5-deficient mice: a possible role for FGF-4 and FGF-6. *Development* **122**, 141-150.

Grifone, R., Demignon, J., Giordani, J., Niro, C., Souil, E., Bertin, F., Laclef, C., Xu, P.-X. and Maire, P. (2007). Eya1 and Eya2 proteins are required for hypaxial somitic myogenesis in the mouse embryo. *Dev. Biol.* **302**, 602-616. doi:10.1016/j.ydbio.2006.08.059

Hasty, P., Bradley, A., Morris, J. H., Edmondson, D. G., Venuti, J. M., Olson, E. N. and Klein, W. H. (1993). Muscle deficiency and neonatal death in mice with a

targeted mutation in the myogenin gene. *Nature* **364**, 501-506. doi:10.1038/364501a0

Hayashi, S., Lewis, P., Pevny, L. and McMahon, A. P. (2002). Efficient gene modulation in mouse epiblast using a Sox2Cre transgenic mouse strain. *Mech. Dev.* **119** Suppl. 1, S97-S101. doi:10.1016/S0925-4773(03)00099-6

Horan, G. S., Ramirez-Solis, R., Featherstone, M. S., Wolgemuth, D. J., Bradley, A. and Behringer, R. R. (1995). Compound mutants for the paralogous hoxa-4, hoxb-4, and hoxd-4 genes show more complete homeotic transformations and a dose-dependent increase in the number of vertebrae transformed. *Genes Dev.* **9**, 1667-1677. doi:10.1101/gad.9.13.1667

Huang, R., Lang, E. R., Otto, W. R., Christ, B. and Patel, K. (2001). Molecular and cellular analysis of embryonic avian tongue development. *Anat. Embryol.* **204**, 179-187. doi:10.1007/s004290100196

Ikeya, M. and Takada, S. (1998). Wnt signaling from the dorsal neural tube is required for the formation of the medial dermomyotome. *Development* **125**, 4969-4976.

Jeannotte, L., Lemieux, M., Charron, J., Poirier, F. and Robertson, E. J. (1993). Specification of axial identity in the mouse: role of the Hoxa-5 (Hox1.3) gene. *Genes Dev.* **7**, 2085-2096. doi:10.1101/gad.7.11.2085

Kessel, M. (1992). Respecification of vertebral identities by retinoic acid. *Development* **115**, 487-501.

Kessel, M. and Gruss, P. (1991). Homeotic transformations of murine vertebrae and concomitant alteration of Hox codes induced by retinoic acid. *Cell* **67**, 89-104. doi:10.1016/0092-8674(91)90574-I

Krumlauf, R. (1994). Hox genes in vertebrate development. *Cell* **78**, 191-201. doi:10.1016/0092-8674(94)90290-9

Lewis, E. B. (1978). A gene complex controlling segmentation in Drosophila. *Nature* **276**, 565-570. doi:10.1038/276565a0

Li, B. and Dewey, C. N. (2011). RSEM: accurate transcript quantification from RNA-seq data with or without a reference genome. *BMC Bioinform.* **12**, 323. doi:10.1186/1471-2105-12-323

Lohnes, D., Kastner, P., Dierich, A., Mark, M., LeMeur, M. and Chambon, P. (1993). Function of retinoic acid receptor γ in the mouse. *Cell* **73**, 643-658. doi:10.1016/0092-8674(93)90246-M

Lohnes, D., Mark, M., Mendelsohn, C., Dolle, P., Dierich, A., Gorry, P., Gansmuller, A. and Chambon, P. (1994). Function of the retinoic acid receptors (RARs) during development (I). Craniofacial and skeletal abnormalities in RAR double mutants. *Development* **120**, 2723-2748.

Madisen, L., Zwingman, T. A., Sunkin, S. M., Oh, S. W., Zariwala, H. A., Gu, H., Ng, L. L., Palmiter, R. D., Hawrylycz, M. J., Jones, A. R. et al. (2010). A robust and high-throughput Cre reporting and characterization system for the whole mouse brain. *Nat. Neurosci.* **13**, 133-140. doi:10.1038/nn.2467

Manley, N. R. and Capecchi, M. R. (1997). Hox group 3 paralogous genes act synergistically in the formation of somitic and neural crest-derived structures. *Dev. Biol.* **192**, 274-288. doi:10.1006/dbio.1997.8765

Mann, R. S. and Affolter, M. (1998). Hox proteins meet more partners. *Curr. Opin. Genet. Dev.* **8**, 423-429. doi:10.1016/S0959-437X(98)80113-5

Marshall, H., Morrison, A., Studer, M., Pöpperl, H. and Krumlauf, R. (1996). Retinoids and Hox genes. *FASEB J.* **10**, 969-978. doi:10.1096/fasebj.10.9.8801179

Martin, M. (2011). Cutadapt removes adapter sequences from high-throughput sequencing reads. *EMBnet J. North Am.* **17**, 10-12. doi:10.14806/ej.17.1.200

McGinnis, W., Levine, M. S., Hafen, E., Kuroiwa, A. and Gehring, W. J. (1984). A conserved DNA sequence in homoeotic genes of the Drosophila Antennapedia and bithorax complexes. *Nature* **308**, 428-433. doi:10.1038/308428a0

McIntyre, D. C., Rakshit, S., Yallowitz, A. R., Loken, L., Jeannotte, L., Capecchi, M. R. and Wellik, D. M. (2007). Hox patterning of the vertebrate rib cage. *Development* **134**, 2981-2989. doi:10.1242/dev.007567

Merabet, S. and Mann, R. S. (2016). To be specific or not: the critical relationship between Hox and TALE proteins. *Trends Genet.* **32**, 334-347. doi:10.1016/j.tig.2016.03.004

Mercader, N., Leonardo, E., Azpiazu, N., Serrano, A., Morata, G., Martínez-A, C. and Torres, M. (1999). Conserved regulation of proximodistal limb axis development by Meis1/Hth. *Nature* **402**, 425-429. doi:10.1038/46580

Mercader, N., Leonardo, E., Piedra, M. E., Martinez, A. C., Ros, M. A. and Torres, M. (2000). Opposing RA and FGF signals control proximodistal vertebrate limb development through regulation of Meis genes. *Development* **127**, 3961-3970.

Mercader, N., Tanaka, E. M. and Torres, M. (2005). Proximodistal identity during vertebrate limb regeneration is regulated by Meis homeodomain proteins. *Development* **132**, 4131-4142. doi:10.1242/dev.01976

Mercader, N., Selleri, L., Criado, L. M., Pallares, P., Parras, C., Cleary, M. L. and Torres, M. (2009). Ectopic Meis1 expression in the mouse limb bud alters P-D patterning in a Pbx1-independent manner. *Int. J. Dev. Biol.* **53**, 1483-1494. doi:10.1387/ijdb.072430nm

Muller, F. and O'Rahilly, R. (1994). Occipitocervical segmentation in staged human embryos. *J. Anat.* **185**, 251-258.

Musumeci, G., Castrogiovanni, P., Coleman, R., Szychlinska, M. A., Salvatorelli, L., Parenti, R., Magro, G. and Imbesi, R. (2015). Somitogenesis: from somite to skeletal muscle. *Acta Histochem.* **117**, 313-328. doi:10.1016/j.acthis.2015.02.011

Nagano, T., Takehara, S., Takahashi, M., Aizawa, S. and Yamamoto, A. (2006). Shisa2 promotes the maturation of somitic precursors and transition to the segmental fate in Xenopus embryos. *Development* **133**, 4643-4654. doi:10.1242/dev.02657

Oulad-Abdelghani, M., Chazaud, C., Bouillet, P., Sapin, V., Chambon, P. and Dollé, P. (1997). Meis2, a novel mouse Pbx-related homeobox gene induced by retinoic acid during differentiation of P19 embryonal carcinoma cells. *Dev. Dyn.* **210**, 173-183. doi:10.1002/(SICI)1097-0177(199710)210:2<173::AID-AJA9>3.0.CO;2-D

Patapoutian, A., Yoon, J. K., Miner, J. H., Wang, S., Stark, K. and Wold, B. (1995). Disruption of the mouse MRF4 gene identifies multiple waves of myogenesis in the myotome. *Development* **121**, 3347-3358.

Penkov, D., San Martín, D. M., Fernandez-Díaz, L. C., Rosselló, C. A., Torroja, C., Sánchez-Cabo, F., Warnatz, H. J., Sultan, M., Yaspo, M. L., Gabrieli, A. et al. (2013). Analysis of the DNA-binding profile and function of TALE homeoproteins reveals their specialization and specific interactions with Hox genes/proteins. *Cell Rep.* **3**, 1321-1333. doi:10.1016/j.celrep.2013.03.029

Pöpperl, H., Rikhof, H., Cheng, H., Haffter, P., Kimmel, C. B. and Moens, C. B. (2000). *lazarus* is a novel pbx gene that globally mediates hox gene function in zebrafish. *Mol. Cell* **6**, 255-267. doi:10.1016/S1097-2765(00)00027-7

Rhinn, M. and Dolle, P. (2012). Retinoic acid signalling during development. *Development* **139**, 843-858. doi:10.1242/dev.065938

Rieckhof, G. E., Casares, F., Ryoo, H. D., Abu-Shaar, M. and Mann, R. S. (1997). Nuclear translocation of extradenticle requires homothorax, which encodes an extradenticle-related homeodomain protein. *Cell* **91**, 171-183. doi:10.1016/S0092-8674(00)80400-6

Ritchie, M. E., Phipson, B., Wu, D., Hu, Y., Law, C. W., Shi, W. and Smyth, G. K. (2015). limma powers differential expression analyses for RNA-sequencing and microarray studies. *Nucleic Acids Res.* **43**, e47. doi:10.1093/nar/gkv007

Rosello-Diez, A., Arques, C. G., Delgado, I., Giovinazzo, G. and Torres, M. (2014). Diffusible signals and epigenetic timing cooperate in late proximo-distal limb patterning. *Development* **141**, 1534-1543. doi:10.1242/dev.106831

Sadate-Ngatchou, P. I., Payne, C. J., Dearth, A. T. and Braun, R. E. (2008). Cre recombinase activity specific to postnatal, premeiotic male germ cells in transgenic mice. *Genesis* **46**, 738-742. doi:10.1002/dvg.20437

Saga, Y., Miyagawa-Tomita, S., Takagi, A., Kitajima, S., Miyazaki, J. and Inoue, T. (1999). MesP1 is expressed in the heart precursor cells and required for the formation of a single heart tube. *Development* **126**, 3437-3447.

Sakai, Y., Meno, C., Fujii, H., Nishino, J., Shiratori, H., Saijoh, Y., Rossant, J. and Hamada, H. (2001). The retinoic acid-inactivating enzyme CYP26 is essential for establishing an uneven distribution of retinoic acid along the anterio-posterior axis within the mouse embryo. *Genes Dev.* **15**, 213-225. doi:10.1101/gad.851501

Sánchez-Herrero, E., Vernós, I., Marco, R. and Morata, G. (1985). Genetic organization of Drosophila bithorax complex. *Nature* **313**, 108-113. doi:10.1038/313108a0

Selleri, L., Depew, M. J., Jacobs, Y., Chanda, S. K., Tsang, K. Y., Cheah, K. S., Rubenstein, J. L., O'Gorman, S. and Cleary, M. L. (2001). Requirement for Pbx1 in skeletal patterning and programming chondrocyte proliferation and differentiation. *Development* **128**, 3543-3557.

Shen, W. F., Montgomery, J. C., Rozenfeld, S., Moskow, J. J., Lawrence, H. J., Buchberg, A. M. and Largman, C. (1997). AbdB-like Hox proteins stabilize DNA binding by the Meis1 homeodomain proteins. *Mol. Cell. Biol.* **17**, 6448-6458. doi:10.1128/MCB.17.11.6448

Tremblay, P., Dietrich, S., Mericskay, M., Schubert, F. R., Li, Z. and Paulin, D. (1998). A crucial role for Pax3 in the development of the hypaxial musculature and the long-range migration of muscle precursors. *Dev. Biol.* **203**, 49-61. doi:10.1006/dbio.1998.9041

Unnisa, Z., Clark, J. P., Roychoudhury, J., Thomas, E., Tessarollo, L., Copeland, N. G., Jenkins, N. A., Grimes, H. L. and Kumar, A. R. (2012). Meis1 preserves hematopoietic stem cells in mice by limiting oxidative stress. *Blood* **120**, 4973-4981. doi:10.1182/blood-2012-06-435800

Vermot, J., Garnier, J.-M., Dierich, A., Niederreither, K., Harvey, R. P., Chambon, P. and Dollé, P. (2006). Conditional (loxP-flanked) allele for the gene encoding the retinoic acid-synthesizing enzyme retinaldehyde dehydrogenase 2 (RALDH2). *Genesis* **44**, 155-158. doi:10.1002/gene.20195

Vinagre, T., Moncaut, N., Carapuço, M., Nóvoa, A., Bom, J. and Mallo, M. (2010). Evidence for a myotomal Hox/Myf cascade governing nonautonomous control of rib specification within global vertebral domains. *Dev. Cell* **18**, 655-661. doi:10.1016/j.devcel.2010.02.011

Vitobello, A., Ferretti, E., Lampe, X., Vilain, N., Ducret, S., Ori, M., Spetz, J.-F., Selleri, L. and Rijli, F. M. (2011). Hox and Pbx factors control retinoic acid synthesis during hindbrain segmentation. *Dev. Cell* **20**, 469-482. doi:10.1016/j.devcel.2011.03.011

Vivian, J. L., Olson, E. N. and Klein, W. H. (2000). Thoracic skeletal defects in myogenin- and MRF4-deficient mice correlate with early defects in myotome and intercostal musculature. *Dev. Biol.* **224**, 29-41. doi:10.1006/dbio.2000.9788

Vlachakis, N., Choe, S. K. and Sagerstrom, C. G. (2001). Meis3 synergizes with Pbx4 and Hoxb1b in promoting hindbrain fates in the zebrafish. *Development* **128**, 1299-1312.

Development (2021) 148, dev193813. doi:10.1242/dev.193813

Waskiewicz, A. J., Rikhof, H. A., Hernandez, R. E. and Moens, C. B. (2001). Zebrafish Meis functions to stabilize Pbx proteins and regulate hindbrain patterning. *Development* **128**, 4139-4151.

Wehn, A. K., Gallo, P. H. and Chapman, D. L. (2009). Generation of transgenic mice expressing Cre recombinase under the control of the Dll1 mesoderm enhancer element. *Genesis* **47**, 309-313. doi:10.1002/dvg.20503

Yashiro, K., Zhao, X., Uehara, M., Yamashita, K., Nishijima, M., Nishino, J., Saijoh, Y., Sakai, Y. and Hamada, H. (2004). Regulation of retinoic acid distribution is required for proximodistal patterning and outgrowth of the developing mouse limb. *Dev. Cell* **6**, 411-422. doi:10.1016/S1534-5807(04)00062-0

Zhang, W., Behringer, R. R. and Olson, E. N. (1995). Inactivation of the myogenic bHLH gene MRF4 results in up-regulation of myogenin and rib anomalies. *Genes Dev.* **9**, 1388-1399. doi:10.1101/gad.9.11.1388